ELEMENTA
Science of the Anthropocene

Lenss, M, et al. 2024. Phytoplankton bloom distribution and succession driven by sea-ice melt in the Kong Håkon VII Hav. *Elem Sci Anth*, 12: 1. DOI: https://doi.org/10.1525/elementa.2023.00122

RESEARCH ARTICLE

Phytoplankton bloom distribution and succession driven by sea-ice melt in the Kong Håkon VII Hav

Megan Lenss[1,2,*], Sebastien Moreau[2,3], Tore Hattermann[2,3], Jozef Wiktor[4], Magdalena Różańska[4], Philippe Claeys[5], Natacha Brion[5], Melissa Chierici[6], Agneta Fransson[2], and Karley Campbell[1]

The existence of ice-edge phytoplankton blooms in the Southern Ocean is well described, yet direct observations of the mechanisms of phytoplankton bloom development following seasonal sea-ice melt remain scarce. This study constrains such responses using biological and biogeochemical datasets collected along a coastal-to-offshore transect that bisects the receding sea-ice zone in the Kong Håkon VII Hav (off the coast of Dronning Maud Land). We documented that the biogeochemical growing conditions for phytoplankton vary on a latitudinal gradient of sea-ice concentration, where increased sea-ice melting creates optimal conditions for growth with increased light availability and potentially increased iron supply. The zones of the study area with the least ice cover were associated with diatom dominance, the greatest chlorophyll *a* concentrations, net community production, and dissolved inorganic carbon drawdown, as well as lower sea surface fugacity of CO_2. Together, these associations imply higher potential for an oceanic CO_2 sink due, at least in part, to more advanced bloom phase and/or larger bloom magnitude stemming from a relatively longer period of light exposure, as compared to the more ice-covered zones in the study area. From stable oxygen isotope fractions, sea-ice meltwater fractions were highest in the open ocean zone and meteoric meltwater fractions were highest in the coastal and polynya zones, suggesting that potential iron sources may also change on a latitudinal gradient across the study area. Variable phytoplankton community compositions were related to changing sea-ice concentrations, with a typical species succession from sympagic flagellate species (*Pyramimonas* sp. and *Phaeocystis antarctica*) to pelagic diatoms (e.g., *Dactyliosolen tenuijunctus*) observed across the study area. These results fill a spatiotemporal gap in the Southern Ocean, as sea-ice melting plays a larger role in governing phytoplankton bloom dynamics in the future Southern Ocean due to changing sea-ice conditions caused by anthropogenic global warming.

Keywords: Phytoplankton, Sea ice, Light, Iron, Seeding, Southern Ocean

1. Introduction

The Southern Ocean accounts for 50% of the oceanic uptake of atmospheric carbon dioxide (CO_2), and 75% of the excess heat generated by anthropogenic CO_2, despite representing only 20% of total ocean surface area (Frölicher et al., 2015; Gregor et al., 2019; Gruber et al., 2019). The disproportionate influx of atmospheric CO_2 into the Southern Ocean is facilitated in part by the biological pump, which is driven by phytoplankton photosynthetic production (e.g., Chierici et al., 2004; Fransson et al., 2004b; Arrigo et al., 2008). Phytoplankton bloom development in the Southern Ocean sea-ice zone (SIZ) is especially enhanced relative to the permanently open-ocean zone due to the influence of sea ice on light availability, via enhanced water column stability, and iron supply in the water column (Smith and Nelson, 1985; Arrigo et al., 2008; Deppeler and Davidson, 2017; Steiner et al., 2021). Strongly seasonal fluctuations in light availability drive the Southern Ocean growing season (Boyd et al., 2000). In early spring and summer when solar radiance is available but sea ice still covers the water column, the penetration of photosynthetically available radiation is largely a function of top-of-sea-ice snow depth and, to a lesser extent, sea-ice thickness (Lancelot et al., 1991; Massom et al., 2001; Joy-Warren et al., 2019). Snow melt and the thinning and breakup of sea ice during the melt season

[1] Arctic and Marine System Ecology, Faculty of Biosciences, Fisheries and Economy, UiT The Arctic University of Norway, Tromsø, Norway

[2] Norwegian Polar Institute, Tromsø, Norway

[3] iC3: Centre for Ice, Cryosphere, Carbon and Climate, Department of Geosciences, UiT The Arctic University of Norway, Tromsø, Norway

[4] Institute of Oceanology, Polish Academy of Sciences, Sopot, Poland

[5] Analytical, Environmental & Geo-Chemistry, Vrije Universiteit Brussel, Brussels, Belgium

[6] Institute of Marine Research, Tromsø, Norway

* Corresponding author:
Email: megan.lenss@npolar.no

facilitate light penetration into the water column and thus trigger pelagic primary production (Schandelmeier and Alexander, 1981; Hague and Vichi, 2021; Horvat et al., 2022). Primary production in the Southern Ocean is regulated secondarily by iron availability, an essential micronutrient for photosynthesis, due to low rates of atmospheric dust input (Martin et al., 1990). In shelf seas around Antarctica, dissolved iron availability is related to melting glaciers, the meltwater pump, sediment entrainment, and warm deep water intrusions onto the continental shelf (St-Laurent et al., 2017; Dinniman et al., 2020). Throughout the Southern Ocean SIZ, sea ice with its associated brines represents a reservoir of iron as it concentrates an elevated amount of both dissolved and particulate iron during its formation that is released into the upper water column during its seasonal melt (Lannuzel et al., 2016). Consequently, the co-occurrence of increased sunlight and relief from iron limitation related to sea-ice melt makes early spring a highly productive season in the Southern Ocean SIZ, as suggested by the well-known occurrence of ice-edge blooms (e.g., Smith and Nelson, 1986; Douglas et al., 2023). However, ice-edge blooms have variable occurrence throughout the Southern Ocean, and their driving processes, hence the role of melting sea ice, are not fully understood (Fitch and Moore, 2007).

Environmental factors associated with sea-ice melt also impact phytoplankton community composition in the SIZ (Kang et al., 2001). Generally, Southern Ocean phytoplankton community composition follows a succession defined by diatom and *Phaeocystis* sp. dominance in the early spring with a shift toward comparatively smaller (3–10 μm) flagellated species in the summer after winter nutrient stocks have been depleted (Davidson et al., 2010). This succession may be impacted by the release of sympagic (ice-associated) algal cells from melting sea ice, which have the potential to fuel phytoplankton bloom development (Smith and Nelson, 1986; Wright et al., 2010). The seeding potential of sea-ice algal communities is hypothesized to be species-specific (van Leeuwe et al., 2022); however, the role of sea ice as a seed inoculum to the water column remains highly debated (e.g., Krell et al., 2005; Selz et al., 2018; van Leeuwe et al., 2020).

Although hypothesized mechanisms for ice-edge blooms are well described in the literature (e.g., Smith and Nelson, 1986; Arrigo et al., 2008; Deppeler and Davidson, 2017; Kauko et al., 2021), direct observations of bloom development during the period of sea-ice retreat remain scarce (von Berg et al., 2020). In this study, we present biogeochemical and oceanographic datasets collected along a coastal-to-offshore transect during the period of sea-ice retreat in the Kong Håkon VII Hav, an understudied region in the Atlantic sector of the Southern Ocean (Vernet et al., 2019). Sampling occurred in early spring (late December to mid-January) during the period of sea-ice breakup and melt. With the resulting data, we studied the relationship between sea-ice melt processes and phytoplankton bloom development and considered the potential growth-limiting factors of light and iron and the seeding potential of sympagic protists. Through this work we sought to fill a spatiotemporal data gap in the Southern Ocean in support of several previously published modeling studies on this topic (e.g., Taylor et al., 2013; Hague and Vichi, 2021; Thomalla et al., 2023).

2. Materials and methods

2.1. Cruise area, water sampling, and laboratory methods

Samples were collected during an oceanographic cruise aboard M/V *Malik Arctica* from December 31, 2020, to January 14, 2021, along two transects: a meridional transect at 6°E and a coastal transect in the region of the Fimbul ice shelf (**Figure 1**; Table S1). The study area was subdivided into four zones based on ship-board observations of sea-ice concentration on each sampling date, following the ASPeCt protocol, as defined in **Table 1** (Beitsch et al., 2015). The threshold of 15% sea-ice concentration was used to define sea-ice presence (Stammerjohn et al., 2008). In this way, this transect represents the various stages of sea-ice retreat that may affect the development of pelagic phytoplankton blooms.

Hydrography of the water column was measured using a conductivity-temperature-depth (CTD) SBE91+ system mounted on an SBE32 carousel water sampler of 12 Niskin bottles. Salinity data were converted to absolute salinity with TEOS-10 (IOC SaI, 2010). Seawater temperature data were used to determine the mixed layer depth (MLD), defined as the depth at which temperature increased by 0.04°C compared to the temperature at 10 m depth, which was determined to be a good indicator of the bottom of the mixed layer based on visual inspection of CTD density profiles measured during sampling (Moreau et al., 2023). Hattermann (2018) was referenced for water mass definitions in the study area, with referenced salinities converted from practical to absolute salinity. Winter water (WW) was defined as water masses with salinities of approximately 34.6 g kg^{-1} and temperatures between −0.5°C and −1.5°C, and warm deep water (WDW) was defined as water masses with salinities of approximately 34.7 g kg^{-1} and temperatures >0°C.

Water samples were collected from a multitude of depths for analyses of chlorophyll *a* (Chl *a*), particulate organic carbon (POC), particulate nitrogen (PN), macronutrient concentrations, the ratio of stable oxygen isotopes in seawater ($\delta^{18}O$), phytoplankton taxonomy, and dissolved inorganic carbon (DIC), and total alkalinity (TA). Samples for Chl *a* were filtered through 0.7 μm GF/F filters (GE Healthcare, Little Chalfont, UK) under low vacuum pressure (approximately −30 kPa), extracted with 100% methanol for approximately 24 hours, and stored at 4°C in the dark (Holm-Hansen and Riemann, 1978). The pigment concentration, including phaeopigments, was measured with a Turner Trilogy Fluorometer, which had been calibrated with Chl *a* standards from Turner Designs (Sunnyvale, California) prior to the cruise. The fluorescence of Chl *a* in the water column (estimated Chl *a*) was also measured in situ with a WETLabs ECO fluorometer in connection with CTD casts and water sampling. Samples for POC and PN analyses were filtered through pre-combusted 25 mm Whatman 0.7 μm GF/F filters

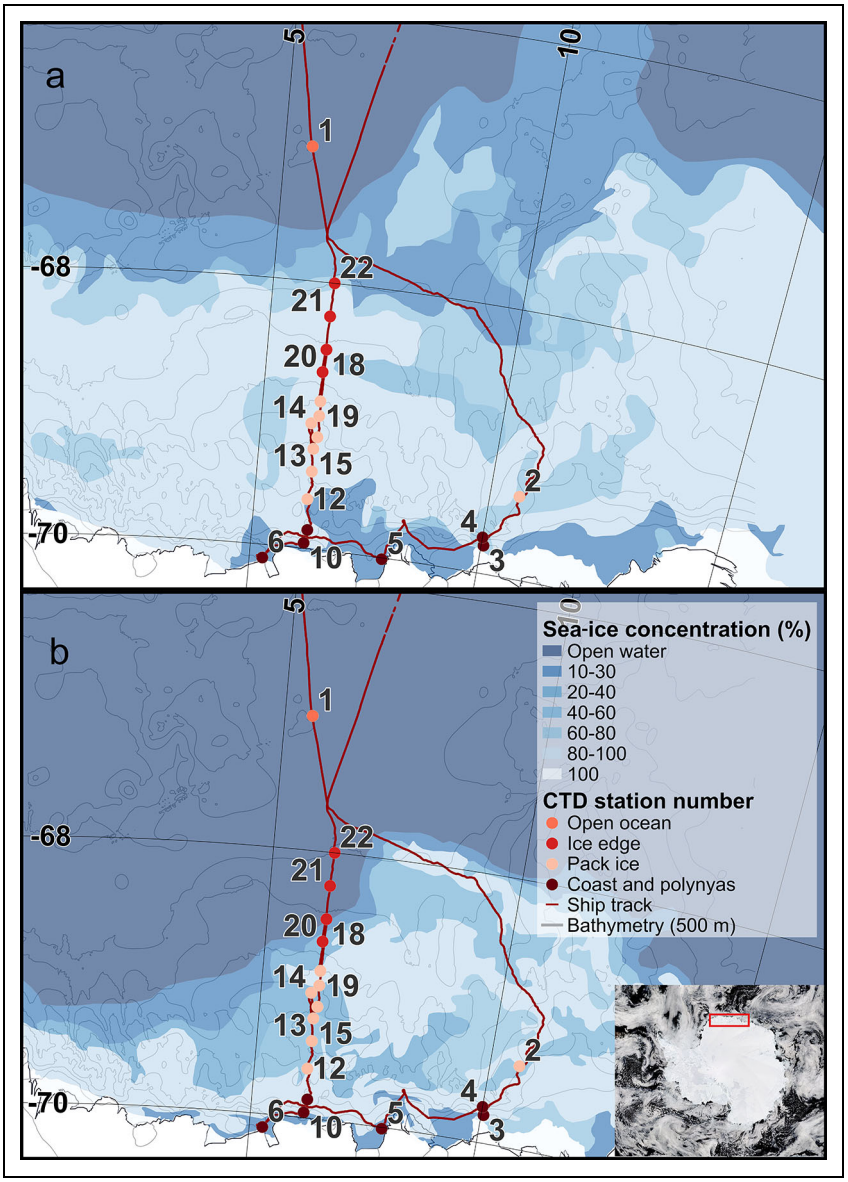

Figure 1. Map of the cruise area in the Kong Håkon VII Hav. The cruise area was focused east of the prime meridian in the Kong Håkon VII Hav. Conductivity-Temperature-Depth (CTD) sampling locations are numbered by station and marked in color based on the subdivision of the study area into four zones according to ship-based observations of sea-ice concentration on each sampling day following the ASPeCt protocol. Sampling efforts were concentrated along a 6°E meridional transect and along the coast of Dronning Maud Land near the Fimbul ice shelf. Sea-ice concentrations are from National Snow and Ice Data Center SIGRID-3 format ice charts. Ice concentrations from January 7, 2021, during the middle of the campaign, are shown in panel a. Ice concentrations from January 28, 2021, one week after the campaign, are shown in panel b to illustrate the observed active sea-ice retreat. On the bottom right is an insert of a MODIS-Terra visible image of Antarctica taken on January 7, 2021 (http://wvs.earthdata.nasa.gov).

(GE Healthcare, Little Chalfont, UK) under low vacuum pressure (approximately −30 kPa; Moran et al., 1999). Samples for POC and PN were stored at −20°C during shipment, then prepared for analysis by drying at 60°C and acidifying in fuming hydrochloric acid. POC and PN concentrations were measured with a coupled element analyzer mass spectrometer (Europa Scientific, ANCA-MS 20-20 15N/13C) at the Tvärminne Zoological Station, Finland. All readings were blank-corrected. Samples for the analysis of macronutrients (nitrate, nitrite, ammonium, phosphate, and silicic acid) were fixed with 200 µL of chloroform and refrigerated at 4°C until standard analysis at the Vrije Universiteit, Brussels, Belgium, using an QuAAtro Autoanalyzer and the spectrophotometric method described by Grasshof et al. (1983). Samples for $\delta^{18}O$ were stored at 4°C in the dark until measurement with a Perspective (Nu Instrument, Ametek) isotope ratio mass spectrometer coupled to a Gas Bench system in the AMGC laboratory at the Vrije Universiteit, Brussels, Belgium (Epstein and Mayeda, 1953; Harmon, 1961). All samples for $\delta^{18}O$ were standardized against V-SMOW, and the standard deviation of the $\delta^{18}O$ analyses was 0.1‰.

Table 1. Overview table of variables by zone defined by sea-ice concentration[a]

Variable	Open Ocean	Ice Edge	Pack Ice	Coast and Polynyas
Percent sea ice (%)	0–15	15–50	>50	Open area in > 50% pack ice
Number of stations	1	4	8	9
Chl a^* (mg m^{-3})[b]	0.473 ± 0.14, $n = 6$	0.238 ± 0.03, $n = 12$	0.538 ± 0.19, $n = 18$	0.391 ± 0.15, $n = 18$
POC* (µg L^{-1})[b]	151 ± 36, $n = 6$	78.2 ±7.3, $n = 19$	91.3 ± 13, $n = 24$	121 ± 26, $n = 26$
POC:Chl *a*	509 ± 140, $n = 6$	412 ± 110, $n = 12$	666 ± 190, $n = 18$	1360 ± 410, $n = 18$
$\delta^{18}O$ (‰)	0.518 ± 0.03, $n = 6$	0.316 ± 0.02, $n = 19$	0.294 ± 0.07, $n = 25$	0.233 ± 0.01, $n = 30$
Meteoric water fraction (‰)	N/A	N/A	0.427 ± 0.62, $n = 29$	3.70 ± 0.81, $n = 21$
Sea-ice meltwater fraction (‰)[c]	4.76 ± 2.3, $n = 6$	−2.04 ± 0.85, $n = 12$	−5.97 ± 0.64, $n = 29$	−4.28 ± 0.85, $n = 21$
NCP* (mmol C m^{-2})[b]	2747, $n = 1$	561.4 ± 130, $n = 2$	627.8 ± 150, $n = 4$	961.2 ± 64, $n = 4$
DIC drawdown (mmol C m^{-2})	3770, $n = 1$	1620 ± 640, $n = 2$	904 ± 190, $n = 4$	882 ± 290, $n = 4$
fCO_2* (µatm)[b]	351.7, $n = 1$	387.7 ± 8.0, $n = 2$	388.3 ± 13, $n = 4$	364.0 ± 7.0, $n = 4$

[a]Data are presented as average ± standard error taken over the upper 100 m per zone; where $n = 1$, no standard error is presented.

[b]An asterisk (*) indicates significant differences between the open ocean and coastal and polynya zones and the ice edge and pack ice zones, with significance considered at the 90% confidence level (i.e., $p < 0.1$) due to low sample sizes.

[c]Negative values of sea-ice meltwater fraction indicate sea-ice growth (Moreau et al., 2019).

Samples for taxonomic analyses by microscopy were collected at selected CTD sampling locations, targeting three samples per station (1–6 stations per zone) from the surface, Chl *a* maximum, and below Chl *a* maximum. Samples were fixed with glutaraldehyde and formaldehyde and thereafter stored at 4°C in the dark. Following the Utermöhl method (Utermöhl, 1958; Edler and Elbrächter, 2010), 50 mL of subsample were poured into Utermöhl sedimentation chambers (HYDRO-BIOS©, Kiel, Germany) and sedimented for 24–40 hours before analysis under a Niko Ti inverted light microscope equipped with phase and Nomarski contrasts and image analysis system (NIS Elements). Identification and counting were performed along transects across the bottom glass of the Utermöhl chamber under 100× magnification for cells bigger than 20 µm and under 400–600× magnification for cells <20 µm. The identification of taxa was carried out based on morphological characteristics following Johansen and Fryxell (1985), Thomas (1997), Scott and Marchant (2005), Cefarelli et al. (2010), and WoRMS Editorial Board (2024). Cells that were damaged, either due to fixation or environmental processes, were classified into higher systematic units or arbitrarily established groups based on size classes.

Water samples for DIC and TA were preserved with 50 µL saturated mercury chloride immediately after sampling and analyzed post-cruise at the Institute of Marine Research, Tromsø, Norway, using potentiometric titration with hydrochloric acid (0.1N) on a Versatile INstrument for the Determination of Titration Alkalinity (VINDTA 3S, Marianda, Germany; Dickson et al., 2007). The DIC was determined using coulometric titration and photometric detection (Johnson et al., 1987) on a Versatile INstrument for the determination of DIC in seawater (VINDTA 3D, Marianda, Germany). The measured values for DIC and TA were corrected against Certified Reference Materials provided by A. G. Dickson, Scripps Institution of Oceanography, USA (Dickson, 2001). The analytical precision for both DIC and TA, as determined from the average standard deviation of four replicate analyses on the Certified Reference Materials, was within ±2 µmol kg^{-1}. The sea surface fugacity of CO_2 (fCO_2) was calculated from TA, DIC, salinity, temperature, and depth as input parameters in the CO2SYS program (Pierrot et al., 2006). The calculations used the carbonate system dissociation constants (K*1 and K*2) estimated by Mehrbach et al. (1973) and modified by Dickson and Millero (1987). The hydrogen sulfate (HSO_4^-) dissociation constant was taken from Dickson (1990). The mean atmospheric fCO_2 value was estimated at approximately 404 µatm using the atmospheric fCO_2 measured in the study region in 2019 and adding a 2 µatm $year^{-1}$ increase rate to calculate for the year 2021 (Ogundare et al., 2021).

2.2. Satellite data

Data from the National Oceanic and Atmospheric Administration's Special Sensor Microwave Imager/Sounder scanning imagers onboard the Defense Meteorological Satellite Program satellites F-16, F-17, and F-18 were obtained from EUMETSAT Ocean and Sea Ice Satellite Application Facilities (OSI SAF, 2017). Downloaded data had a spatial resolution of 25 km and were used to estimate daily sea-ice concentration from 2020 to 2021 using the SICCI2LF algorithm (Lavergne et al., 2019). Ice charts (**Figure 1**) were made using the U.S. National Ice Center Arctic and Antarctic Regional Sea Ice Charts in SIGRID-3 dataset G10013, obtained from the National Snow and Ice Data Center (U.S. National Ice Center, 2022).

2.3. Data analysis

Data analyses were conducted with Matlab R2019b. Maps were built on QGIS (v. 3.20.0) using Quantarctica (Matsuoka et al., 2021) and on Matlab using the m_map package as downloaded online from the University of British Columbia Department of Earth, Ocean and Atmospheric Sciences in November 2021.

The in situ fluorescence data were calibrated with the concurrent Chl *a* samples extracted from discrete water samples. A linear fit was calculated using the dark value at depth (100–500 m depths) and the median of upcast values in a 2 m window at the discrete sample depth to obtain a calibration equation ($y = 0.0895x$, $R^2 = 0.56$). The equation was used to calibrate the downcast values, which was assumed to be most representative of the undisturbed water column, and was used for further analysis. At high light intensities the surface fluorescence signal can be affected by algal non-photochemical quenching, which can damage or down-regulate photosystem II and lower the proportion of absorbed light that is emitted as fluorescence (Öquist et al., 1992; Szmytkowski et al., 2011). Due to the absence of coinciding light backscattering profiles, Chl *a* fluorescence profiles were not corrected for non-photochemical quenching in daytime profiles, meaning that surface florescence values may be underestimates and should be considered with caution (Xing et al., 2018). However, all fluorescence profiles were collected during daytime sunlight conditions and are hence comparable with each other.

Temperature, salinity (absolute salinity, TEOS-10), and macronutrient data were used to calculate net community production (NCP). NCP since the beginning of the production season was estimated from nitrate drawdown integrated from 100 m depth to the surface. Drawdown was calculated by subtracting measured nitrate concentrations in the upper water column (<100 m) from nitrate concentration at 100 m depth, taken as a proxy for WW layer (Fransson et al., 2004b; Moreau et al., 2013). Integrated nitrate drawdown results were further transformed to carbon using Redfield ratios (C:N = 106:16) to give a final estimate of NCP (Redfield et al., 1963). Integrated DIC drawdown from the beginning of the production season was calculated similarly, by subtracting from WW DIC values (using DIC concentrations measured at 100 m depth as proxy) and integrating from 100 m to the surface (Fransson et al., 2004a; Keppler et al., 2020). These values were compared with NCP values to evaluate other potential sources or sinks of DIC, such as air-sea exchange. The beginning of the production season was assumed as December 1 for estimates of both NCP and DIC drawdown rate based on the timing of known bloom initiation in the Kong Håkon VII Hav and surrounding areas as gathered from both observational and long-term (1997–2020) remote sensing data (e.g., Kauko et al., 2021).

The fractions of sea-ice melt and meteoric water (originating from direct precipitation into the ocean or the melting of glacial ice) were estimated following the protocols of Meredith et al. (2013) and Silvano et al. (2018) using salinity and $\delta^{18}O$ as conservative tracers. The fractions of sea-ice melt and meteoric water were interpreted as proxies for sea-ice and glacial iron sources, respectively (Moreau et al., 2019). Salinity and $\delta^{18}O$ values for WW were chosen to be 34.4 and −0.28‰, respectively, based on observations during the campaign. Salinity (6.2 g kg^{-1}) and $\delta^{18}O$ (2.1‰) values for sea ice were taken from values published in Silvano et al. (2018). Salinity of meteoric water was set to zero, and −30‰ was chosen for $\delta^{18}O$ of meteoric water, an intermediate value for meteoric water based on the range presented by Silvano et al. (2018).

Statistical testing to determine the significance of difference between zones was tested for measured Chl *a*, POC, NCP, and fCO_2 using the Statistics and Machine Learning Toolbox in Matlab. Subgroups within the data for statistical testing were defined as zones with elevated Chl *a* concentrations (open ocean and coastal and polynya zones) and zones with low Chl *a* concentrations (ice edge and pack ice zones). Significance was tested using the non-parametric Mann Whitney *U* test after non-normality was determined via Kolmogorov-Spearman test. Significance was considered at the 90% confidence level (i.e., $p < 0.1$) due to small sample sizes. A canonical correlation analysis was also performed using R Studio (version 2021.09) to evaluate the relationships between species distribution and environmental parameters (i.e., temperature, salinity, MLD, nitrate, $\delta^{18}O$, etc.).

3. Results

3.1. Oceanography across the study area

Prior to the cruise, the ice edge was located immediately south of Station 1 (**Figure 1a**) on the 6°E transect. Rapid southward sea-ice retreat occurred throughout the study period. On January 7, 2021, the sea-ice cover over most station sites was >80% (**Figure 1a**), and by January 28, 2021, the sea-ice cover over the study area was <60% at most station sites (**Figure 1b**). The study area was not completely ice-free until the end of February, roughly 4 weeks after the campaign was completed (not shown). Ice charts in SIGRID-3 format (WMO-IOC, 2004) indicate weekly ice concentration on a 10 km × 10 km gridded format (**Figure 1a** and **b**) and provide relatively coarse concentration data compared to ship-board observations used to define zones across the study area (**Table 1**).

Surface waters (taken at 10 m depth) across the entire study area were generally cold (<0°C) and fresh (34.11–34.40 g kg^{-1}; **Figure 2a** and **b**). The maximum surface temperature (−0.49°C) was observed in the open ocean zone (Station 1), and slightly higher sea surface temperatures, as compared to the other zones, were also observed in the coast and polynyas zone (−1.60°C to −1.24°C). The coldest sea surface temperatures were observed in the pack ice zone (−1.72°C to −1.57°C). The maximum sea surface salinity (34.40 g kg^{-1}) was observed in the open ocean zone (Station 1), which is slightly fresher than WW in this region. The lowest sea surface salinities (34.11–34.34 g kg^{-1}) were fresher than WW and were observed in the pack ice zone. Generally, the ice-covered zones (ice edge and pack ice zones) displayed colder and fresher sea surface properties than the zones with more open water (open ocean and coastal and polynya zones).

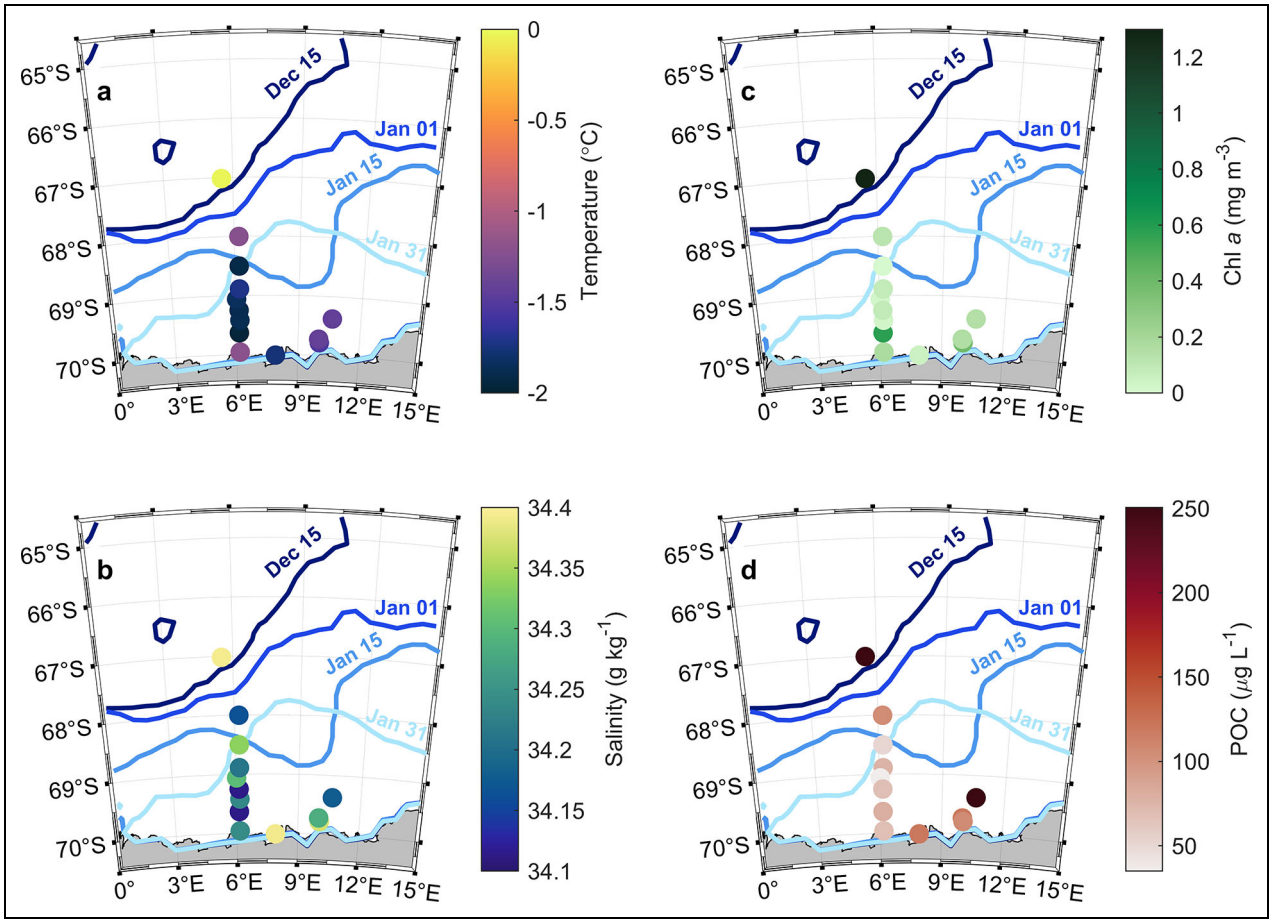

Figure 2. Maps showing sea surface properties throughout the study area. Sea surface properties shown here are taken at 10 m depth, and blue contours represent the receding ice edge, calculated as 15% ice concentration using data downloaded from EUMETSAT DMSP satellites F-16, F-17, F-18. The small circle from the December 15 ice contour in the upper left of the maps shows a drifting patch of sea ice. The Antarctic continent is shaded in gray, and overlapping ice contours along the continent demarcate the southern termination of the sea ice along the coast. (a) Sea surface temperature and (b) salinity were measured using a SBE911+ CTD; measured concentrations of sea surface (c) chlorophyll *a* (Chl *a*) and (d) POC were derived from filtered seawater samples.

Water column properties over the upper 100 m across the 6°E transect are detailed in **Figure 3**. Here, water column temperatures were higher in the northern end of the transect than in the south. There was a deep (>70 m), warm, and saline water mass at the north end of the transect, consistent with WDW in this region. A cold (<−1.5°C) water mass was observed below the mixed layer in the middle of the transect between 68°S and 69.5°S. The water in the mixed layer was generally warmer and fresher than water at depth across the transect, and the freshest water (<34.1 g kg^{-1}) was observed in the mixed layer in the ice edge zone.

3.2. Phytoplankton biomass and primary production

The Chl *a* concentrations ranged from undetectable to 2.78 mg m^{-3} across the entire study area. Significantly higher concentrations of Chl *a* were observed in the open ocean and coastal and polynya zones as compared to the ice edge and pack ice zones ($p = 0.03$; **Figures 2c** and **3c**; **Table 1**). In the open ocean zone, elevated Chl *a* was observed below the MLD until about 40 m, with a maximum of 0.91 mg m^{-3}. In the ice edge zone, Chl *a* concentrations were low (<0.50 mg m^{-3}). Station 12 had elevated levels of Chl *a* (2.78 mg m^{-3}) and could be considered an outlier, as all other stations in the pack ice zone had low levels of measured Chl *a* (<0.4 mg m^{-3}). In the coastal and polynya zones, high concentrations of estimated Chl *a* were recorded below the MLD between 25 m and 60 m, and a local maximum of 2.04 mg m^{-3} was measured at Station 10.

The POC trends followed the general Chl *a* trends, with significantly higher concentrations in the open ocean and coastal and polynya zones as compared to the pack ice and ice edge zones ($p = 0.08$; **Figure 2d**). Average POC concentrations ± standard error in the upper 100 m of the water column were 151 ± 36 μg L^{-1} ($n = 6$), 78.2 ± 7.3 μg L^{-1} ($n = 19$), 91.3 ± 13 μg L^{-1} ($n = 24$), and 121 ± 26 μg L^{-1} ($n = 26$) for the open ocean, ice edge, pack ice, and coastal and polynya zones, respectively (**Table 1**). Maximum POC concentrations in the open ocean and ice edge zones were 250 μg mL^{-1} and 156 μg mL^{-1}, respectively. The average POC in the pack ice zone was the lowest of all the zones, despite an outlying local maximum of 250 μg mL^{-1} at Station 2. The maximum POC

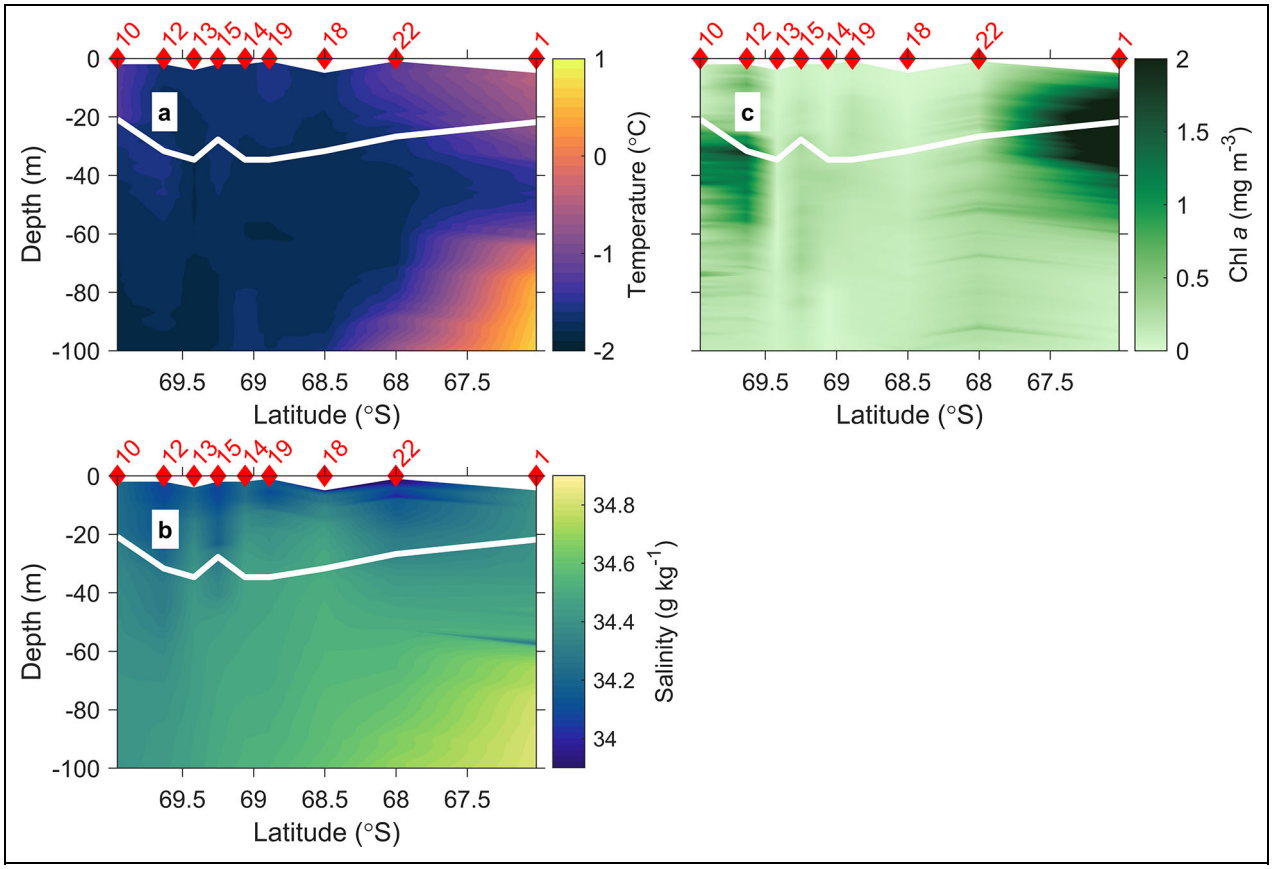

Figure 3. Water column properties in the upper 100 m along the 6°E meridian. In north-south conductivity-temperature-depth (CTD) transects along the 6°E meridian (**Figure 1**), CTDs are labeled with red diamonds across the top and numbered by station. (a) Temperature, (b) salinity, and (c) chlorophyll *a* (Chl *a*) concentrations from calibrated in situ fluorescence profiles are shown for the upper 100 m of the water column, with a white contour representing the depth of the mixed layer based on a temperature increase of 0.04°C relative to the temperature at 10 m depth.

concentration in the upper water column was 753 µg mL^{-1} in the coastal and polynya zone.

Trends in NCP and DIC drawdown were also largely consistent with the distribution of Chl *a* and POC. The NCP rate estimates ranged from 70.0 mmol C m^{-2} to 2750 mmol C m^{-2} from the beginning of the production season (about 6 weeks), with the highest value calculated for the open ocean zone and the lowest for the pack ice zone (**Figure 4a**). Average NCP for each zone was 2750 ($n = 1$), 561 ± 130 ($n = 2$), 627 ± 150 ($n = 4$), and 961 ± 64 mmol C m^{-2} ($n = 4$) for the open ocean, ice edge, pack ice, and coastal and polynya zone, respectively (**Table 1**). The NCP in the open ocean and coastal and polynya zones was significantly higher than the NCP in the ice edge and pack ice zones ($p = 0.01$). Integrated DIC drawdown values were also calculated from the beginning of the production season (about 6 weeks) and ranged from 99 mmol C m^{-2} in the coast and polynyas to 3766 mmol C m^{-2} in the open ocean (**Figure 4b**). Average DIC drawdown for each zone was 3770 ($n = 1$), 1620 ± 640 ($n = 2$), 904 ± 190 ($n = 4$), and 882 ± 290 mmol C m^{-2} ($n = 4$), respectively, for the open ocean, ice edge, pack ice, and coastal and polynya zones (**Table 1**).

There were no significant differences in DIC drawdown in the open ocean and coastal and polynya zones compared to the ice edge and pack ice zones ($p > 0.1$). However, the rates of NCP and DIC drawdown correlated significantly to each other ($R^2 = 0.629$ and $p < 0.01$; Figure S1), despite representing slightly different processes. The potential for air-sea CO_2 gas exchanges was explored using fCO_2 (**Figure 4c**). In general, the calculated values of ocean fCO_2 indicated undersaturation relative to atmospheric CO_2 levels across the entire study area, with fCO_2 between 347 µatm and 410 µatm and a mean value of 376 ± 110 µatm ($n = 11$). The highest calculated fCO_2 values were just above atmospheric values (taken at 404 µatm; Ogundare et al., 2021) and located in the pack ice zone, while the lowest (largest undersaturation) were in the coastal and polynya zone. Trends in fCO_2 across the study area were counter to trends in primary production, with zones of elevated Chl *a* and NCP associated with fCO_2 minima (**Table 1**). Indeed, significantly larger amounts of NCP in the open ocean and coastal and polynya zones ($p = 0.01$) were correlated to significantly lower fCO_2 and more intense CO_2 undersaturation in the sea surface in these zones ($p = 0.07$).

3.3. Potential meltwater sources

The largest fraction of meteoric water (0.007) was observed in the coastal and polynya zone with a positive signal measured to 300 m depth (**Figure 5a**; **Table 1**). A smaller fraction of 0.005 meteoric water was observed in

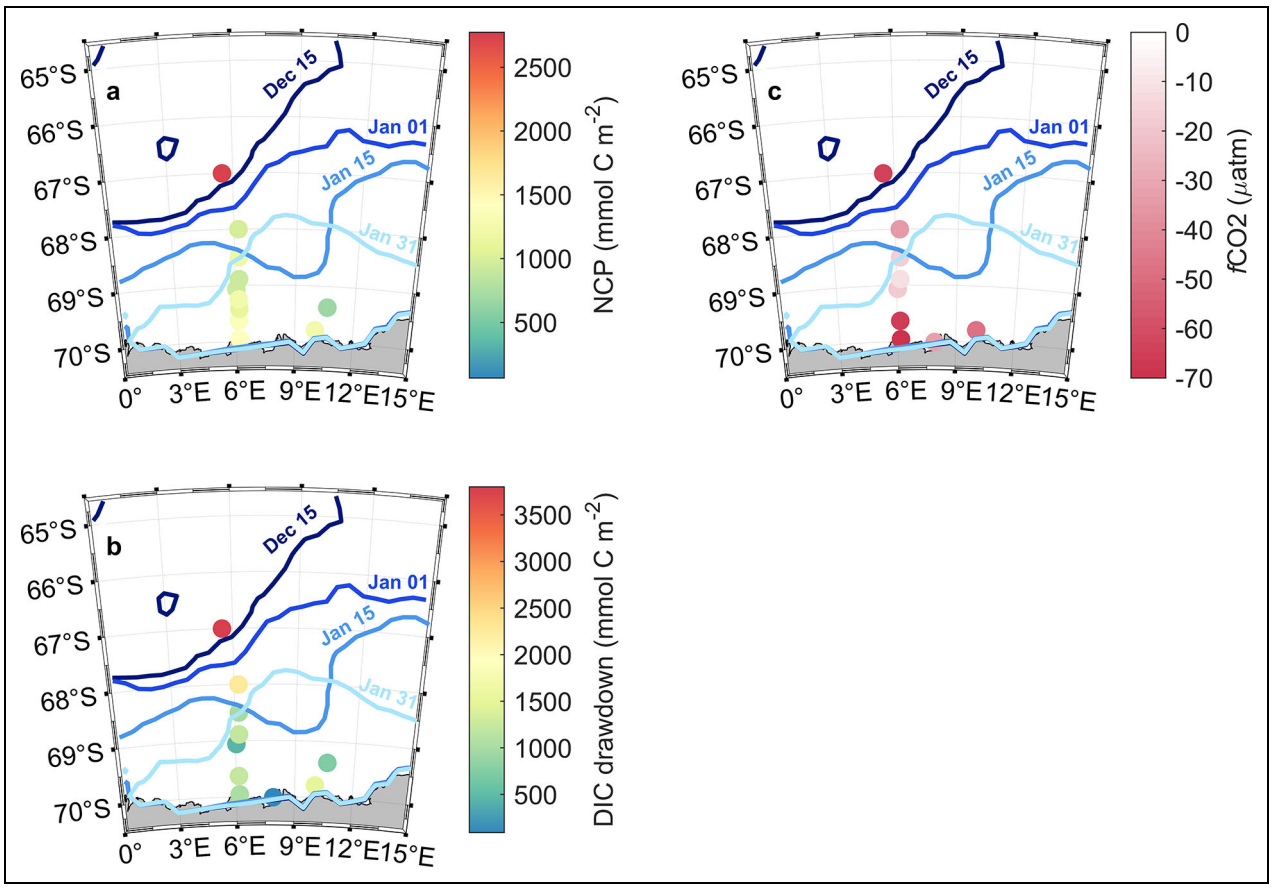

Figure 4. Net community production integrated dissolved inorganic carbon drawdown, and fCO_2 throughout the study area. In maps showing (a) net community production (NCP), (b) integrated dissolved inorganic carbon (DIC) drawdown, and (c) the sea surface fugacity of CO_2, blue contours represent the receding ice edge, calculated as 15% ice concentration using data downloaded from EUMETSAT DMSP satellites F-16, F-17, F-18. The small circle from the December 15 ice contour in the upper left of the maps shows a drifting patch of sea ice. The Antarctic continent is shaded in gray, and overlapping ice contours along the continent demarcate the southern termination of the sea ice along the coast. NCP estimated from nitrate drawdown and both nitrate and DIC drawdown were integrated through the upper 100 m of the water column and transformed into carbon units using the Redfield ratio (Redfield et al., 1963; Moreau et al., 2013). Sea surface fugacity of CO_2 was calculated from DIC and total alkalinity measurements at each CTD location following the method of Zeebe and Wolf-Gladrow (2001).

the pack ice zone until approximately 50 m depth. There was no evidence for meteoric water influence in the ice edge and open ocean zones. In comparison, there was a positive fraction of sea-ice meltwater in all zones except in the coastal and polynya (**Figure 5b**; **Table 1**). The largest fraction of sea-ice meltwater was observed in the ice edge zone (0.023), which also correlated with low (<34.4 g kg^{-1}) sea surface salinities (**Figure 2b**).

3.4. Phytoplankton community composition

The results of the phytoplankton community composition in each zone at the functional group level are summarized in **Figure 6**. The phytoplankton community of the open ocean zone was dominated by diatoms (75%), with *Fragilariopsis nana* (pennate diatom, 28%) and *Dactyliosolen tenuijunctus* (centric diatom, 9%) representing the most dominant species. In the ice-covered zones south of the open ocean zone, diatom abundance decreased while flagellated cells dominated communities, with the total relative abundance amounting to 62%–79% of the community in the ice edge, pack ice, and coastal and polynya zones. At the ice-edge, 39% of the flagellate community was composed of heterotrophic *Choanoflagellatea* indet. In the pack ice and coastal and polynya zones, the flagellate community was dominated by the typical Southern Ocean combination of *Pyramimonas* sp. and *Phaeocystis antarctica*, which together make up 21% and 32% of the communities in those zones, respectively. The pennate diatom species *F. nana* was present in varying abundance throughout the entire study area. A canonical correlation analysis to explore the environmental drivers of species distribution was not able to explain more than 40% of the variance in the dataset and is therefore not presented here.

4. Discussion

4.1. Light limitation of phytoplankton growth

The open ocean and coastal and polynya zones were the zones with the least sea-ice cover and the highest Chl *a*, POC, and NCP (**Figures 1a**, **3c**, and **4a**; **Table 1**). Sea-ice cover is a primary driver of light limitation of

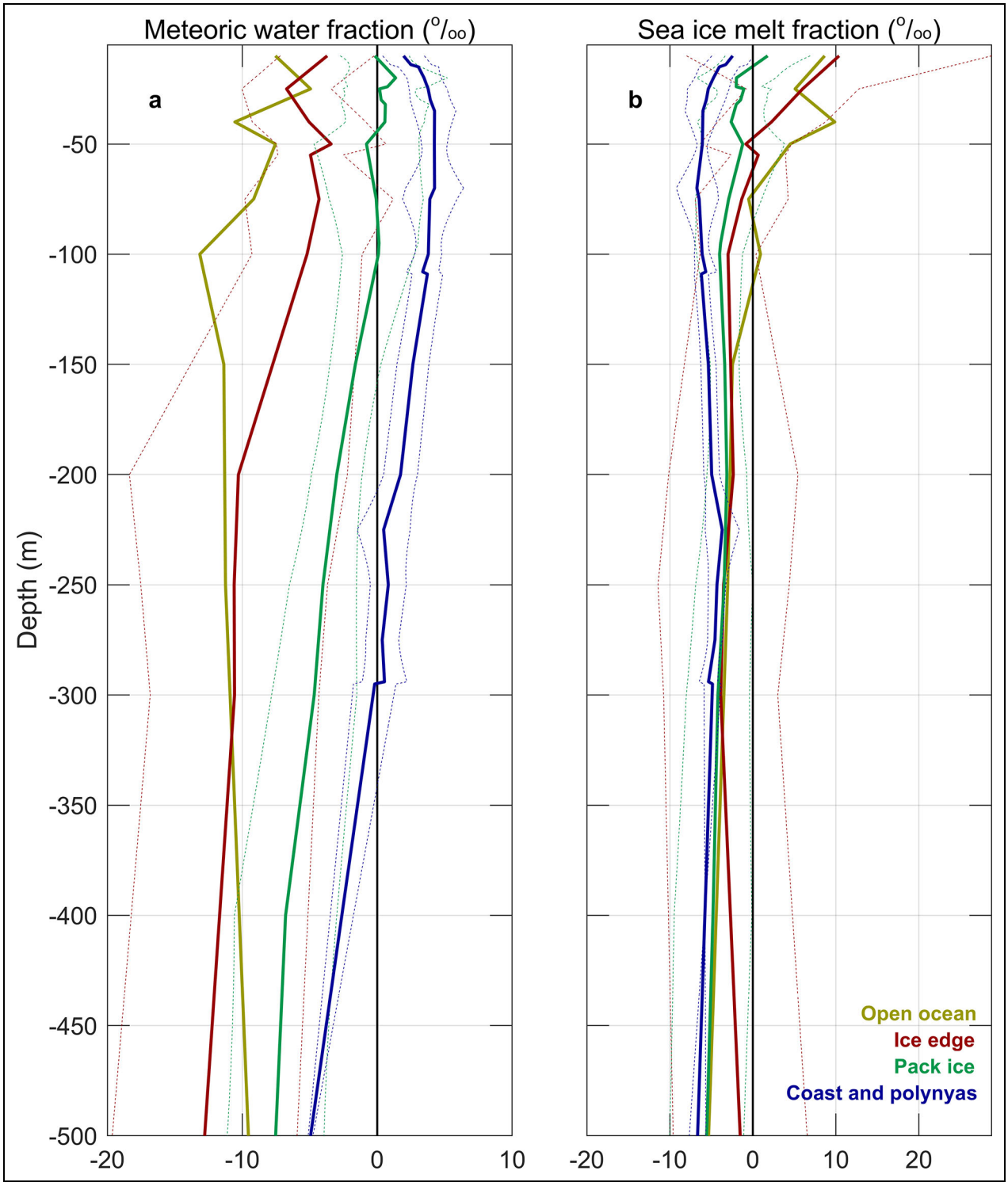

Figure 5. Calculated meteoric and sea-ice meltwater fractions based on salinity and $\delta^{18}O$. Average (± standard deviation) fractions of (a) meteoric water and (b) sea-ice meltwater, determined from salinity and $\delta^{18}O$ observations and published values from Silvano et al. (2018). The open ocean zone does not show a standard error because only one CTD was taken in this zone.

phytoplankton in the Kong Håkon VII Hav (Hague and Vichi, 2021; Kauko et al., 2021), implying that the zones with the least ice cover were the least light-limited during the campaign. The thinning and breakup of sea ice that occurred prior to the campaign in these zones would have enabled greater light penetration into the water column, potentially facilitating earlier photosynthesis than in those zones that remained ice-covered throughout the austral spring. These findings are consistent with previous studies in the Southern Ocean where light has been documented as a primary control on the timing and magnitude of spring phytoplankton bloom development with longer light exposure being correlated with greater NCP (Fransson et al., 2004b; Joy-Warren et al., 2019).

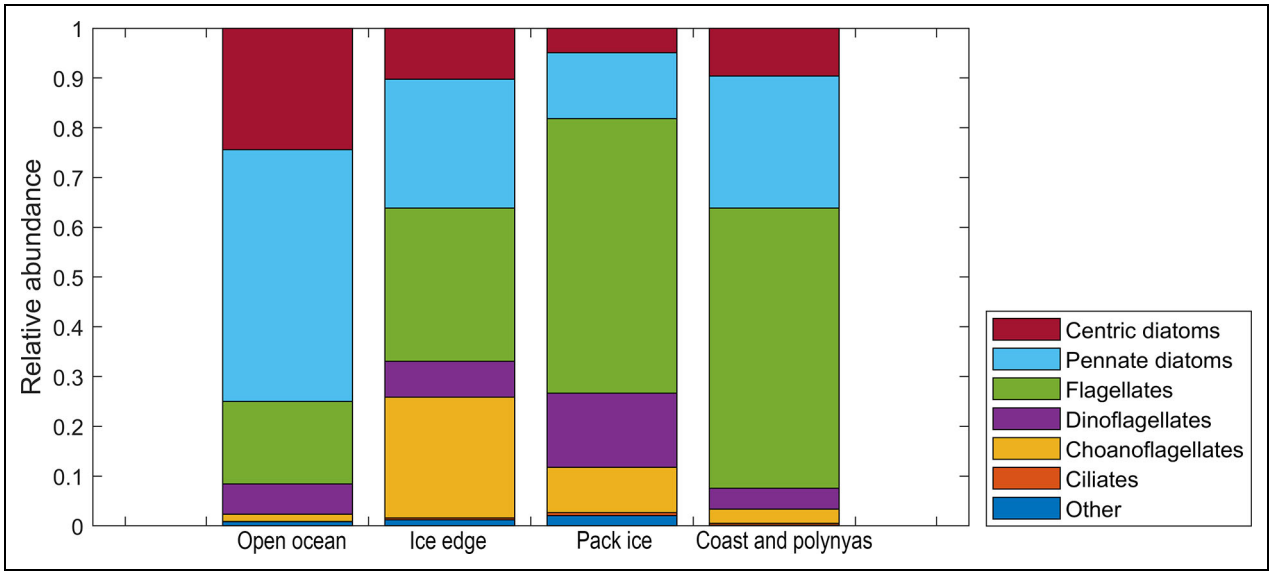

Figure 6. Relative abundance of different protist groups in each zone defined by sea-ice concentration. Protist groups were determined by morphological characteristics during analysis by microscopy. Relative abundance was calculated by summing the number of organisms in a protist group from all locations sampled within a given zone (see Section 2.1) and dividing by the total number of protists summed from the same samples within that zone.

Sea-ice melt also works to concentrate phytoplankton cells in the euphotic zone through the formation of a strong, shallow pycnocline created by a superficial meltwater lens (Moreau et al., 2019). This stabilization of the water column results in an MLD shallower than the euphotic depth and is the proximal cause of phytoplankton bloom development when light penetration is high and nutrient levels are non-limiting and of at least equal importance in creating the conditions for bloom development (Vernet et al., 2019). Indeed, the large provinces of the Southern Ocean that remain ice-free year-round and thus do not experience this stabilization generally show low rates of production per unit area (Arrigo et al., 2008). To estimate the euphotic depth for comparison with the MLD in this study area, a post-factum relationship between sea surface Chl *a* and euphotic depth was used due to the absence of a PAR sensor on the CTD-rosette during this campaign. This relationship was derived from a relatively large historical dataset of Chl *a* in the sea-ice influenced waters off the West Antarctic Peninsula and, because this method was developed using satellite ocean color data, the relationship is only applicable in waters that are not covered by sea ice (Dierssen et al., 2000). Estimated to the 2% light level, the euphotic depth was calculated as 62 ± 18 m ($n = 2$) in the open ocean and 95 ± 11 m ($n = 6$) in the coast and polynyas zone. Therefore, the euphotic depth was >40 m deeper than the MLD in the open ocean and coastal and polynya zones during the campaign, suggesting that phytoplankton would be concentrated within the euphotic layer with sufficient light availability.

The DIC drawdown was higher than NCP at every station except for Stations 3 and 10 (in the coastal and polynya zone; Figure S1), indicating that carbon was in excess and nitrogen was more limiting for primary production. Although this relationship is potentially weakened by the singularity of Station 1 and Figure S1 and should thus be considered with caution, we contend that similar stations in the open ocean zone where light limitation was relieved earliest (due to earlier sea-ice retreat) would render similar results and possibly strengthen the relationship. Our contention is supported by satellite observations during the sampling period suggesting that there was an active bloom in the region with Chl *a* concentrations around 2 μg L^{-1} (data not shown). The NCP was consistent with Chl *a* and POC concentrations throughout the study area, despite estimation by a method that considers only nitrate as a potential nitrogen source. Other nitrogen sources such as ammonium or nitrogen from recycled organic matter were also likely present in the study area, and thus these NCP calculations may be underestimates (Mdutyana et al., 2020; Alkire and Riser, 2023). Additionally, DIC dynamics are highly influenced by CO_2 gas exchanges and other physical processes such as mixing and advection, indicating that DIC cannot be considered representative of biological uptake alone (Chierici et al., 2004). This potential underestimate in NCP together with physical DIC exchanges may explain why DIC drawdown was greater than NCP at most stations. The greatest potential for sea surface CO_2 uptake was observed in the open ocean and coastal and polynya zone and was consistent with evidence of high biological activity (e.g., Chl *a* concentrations and NCP values; **Figure 4c**) and also in alignment with previous findings along the coast in this region (Ogundare et al., 2021). Furthermore, Takahashi et al. (1993) calculated that fCO_2 increases by 4.23% per degree Celsius increase in temperature. This relationship suggests that an increase in fCO_2 of approximately 15 μatm, related to localized surface warming due to seasonal increases in incoming solar radiation in the open ocean zone, was compensated by biological CO_2 drawdown (**Figures 2a** and **4c**). Rates of DIC drawdown greater

than rates of NCP combined with sea surface undersaturation of fCO_2 provide further evidence for bloom development in the open ocean and coastal and polynya zones.

While primary production was greater in zones of lowest sea-ice concentration, POC:Chl *a* ratios suggest that phytoplankton growth began beneath the ice prior to complete ice retreat. Photosynthetic activity underneath compact sea ice in spring and summer has been observed throughout the Southern Ocean, and bloom initiation is suggested to begin 4–5 weeks before complete sea-ice retreat due to extreme low light adaptation strategies by Southern Ocean phytoplankton (Hague and Vichi, 2021; Horvat et al., 2022). Blooms following the ice edge due to relief of light limitation may therefore be in a more intermediate to advanced bloom stage. The ratio POC:Chl *a* can be used to describe the phase of the bloom via the relative proportion of organic material to autotrophic pigmentation, where POC:Chl $a < 100$ indicates living phytoplankton, $100 <$ POC:Chl $a < 200$ indicates phytoplankton-dominated particulate organic matter, and POC:Chl $a > 200$ indicates detrital or degraded organic matter (Liénart et al., 2016; Thomalla et al., 2017; Ratnarajah et al., 2022). In the pack ice zone, the majority of stations (except Stations 2 and 19) had POC:Chl *a* ratios < 100, indicating an active bloom. We note that Station 2 had high POC (250 μg mL^{-1}) and exceptionally high POC:Chl *a* (1850) values compared to the other stations in the pack ice zone (**Figures 2** and S1; **Table 1**). Such high values are not frequently observed above 100 m depth in the water column and were likely caused by the outlying POC concentration in combination with relatively low Chl *a* (0.161 mg m^{-3}). High POC:Chl *a* ratios may also be indicative of an ice algal export event (Ratnarajah et al., 2022), as evidenced by relatively high phaeopigment to total Chl *a* concentrations at Station 2 (average 39.3 ± 4.2%; Tison et al., 2017; Corkill et al., 2023) and large pieces of ice algae found in deep Niskin bottles and stuck to the CTD-Rosette during sampling. Only one station (Station 10) in the remaining study area (i.e., open ocean, ice edge, and coastal and polynya zones) had POC:Chl *a* ratios < 100 to suggest living phytoplankton, and average ratios in the open ocean and coastal and polynya zone were high, 509 ± 140 ($n = 6$) and 660 ± 190 ($n = 18$), respectively (Figure S2; **Table 1**). Average POC:Chl *a* in the ice edge zone was 412 ± 110 ($n = 12$), although POC:Chl $a <$ 200 was observed from samples between 50 m and 55 m depth, potentially indicting a small depth-restricted community of phytoplankton (Figure S2; **Table 1**).

From this understanding, the zones with highest Chl *a* and NCP (open ocean and coastal and polynya zones) had the highest amounts of non-phytoplankton POC in the upper 100 m of the water column, thus suggesting a more advanced bloom phase. In contrast, the zone with the highest amount of Chl *a* relative to other organic material was the pack ice zone, where sea-ice concentration was highest, suggesting that photosynthetic activity was indeed occurring below the ice. Results from taxonomic analyses support a more advanced bloom phase in the open ocean zone and early bloom development in the pack ice zone. The phytoplankton community in the pack ice zone was mostly autotrophic flagellates, especially *Phaeocystis antarctica* and *Pyramimonas* spp., which are typical species for an early spring phytoplankton assemblage in the Southern Ocean, while the open ocean zone community was dominated by diatoms, which are known to more dominant in the later phase of blooms (**Figure 6**; van Leeuwe et al., 2020).

4.2. Potential sources of iron across study zones

Although other micronutrients, such as manganese or vitamin B12, can be limiting for phytoplankton growth (e.g., Moore et al., 2013), iron has long been established as the primary limiting nutrient for phytoplankton growth in the Southern Ocean (e.g., Martin et al., 1990; de Baar et al., 1995; Boyd et al., 2000). High concentrations of iron have been documented in Southern Ocean sea ice, with wide acceptance that sea-ice meltwater contributes bioavailable iron to surface waters (Lannuzel et al., 2016; Vernet et al., 2019; Singh et al., 2023). Also documented is that iron provided from glacial meltwater sources fuels phytoplankton blooms around coastal Antarctica, suggesting that meltwater runoff from the Antarctic ice sheet is another important iron reservoir for phytoplankton growth (e.g., Gerringa et al., 2012; Death et al., 2014). Thus, we discuss potential sources of iron to the study area using calculated meltwater fractions from both sea-ice and meteorologic (glacial) iron sources using $\delta^{18}O$, temperature, and salinity data. As samples for iron measurements were not taken during this study, no direct data on iron concentrations in the water column can be provided, limiting this discussion to potential supply dynamics. However, observed bloom conditions and Chl *a* concentrations indicate that iron concentrations were sufficient to facilitate phytoplankton growth at the time of sampling.

We expect that iron provision from sea ice was a factor during the time of the campaign given the high fractions of sea-ice meltwater present in the open ocean and ice edge zones (**Figure 5b**; **Table 1**). The fractions of sea-ice meltwater that we calculated are high compared to sea-ice meltwater fractions observed on the Sabrina Coast in East Antarctica by Silvano et al. (2018) and in alignment with values presented by Moreau et al. (2019) from East Antarctic polynyas. Here, the maximum sea-ice meltwater fraction calculated was 0.023 (Station 10), while maximum values were approximately 0.003 and approximately 0.030 from Silvano et al. (2018) and Moreau et al. (2019), respectively. Relatively high sea-ice meltwater fractions are a consistent feature of the study area and are well explained by persistent easterly winds resulting in southward Ekman transport and consequential accumulation of sea-ice meltwater (Thompson et al., 2018). We note that the signatures for sea-ice meltwater in salinity persist as conservative tracers over longer time scales than iron is typically present in the water column, which may cause a discrepancy between when the iron was provided and consumed and when we observed the meltwater content (Sherrell et al., 2015). Nevertheless, the evidence for bloom conditions in the open ocean zone indicates more growth than loss, suggesting that phytoplankton cells

were not limited by iron at the time of sampling (Behrenfeld et al., 2017).

The largest source of meteoric water in the study area is expected to originate from basal melting of the ice shelves that fringe the coast of Dronning Maud Land (Ice Shelf Water), in addition to meltwater from drifting icebergs (e.g., Duprat et al., 2016; Herraiz-Borreguero et al., 2016). High meteoric water fractions, especially in the coastal and polynya zone, indicate that glacially derived iron may be an important iron source in the study area (**Figure 5a**; **Table 1**). Compared to the coastal and polynya, the other zones in the study area do not show strong positive signals for meteoric water, indicating that sea-ice meltwater may have played a more dominant role in iron supply than meteoric water in these areas. In addition, atmospheric deposition of iron from precipitation is known to play only a minor role at these latitudes (Jickells and Moore, 2015), rendering sea-ice meltwater and glacial sources as relatively more important in providing iron to phytoplankton in the study area.

Elevated temperatures (1°C) at relatively shallow (approximately 120 m) depth north of the ice pack highlight the presence of WDW (**Figure 1b**), which is known to be upwelled in this region due to wind-driven divergence (Marinov et al., 2006). This presence may represent an additional mechanism of iron supply to phytoplankton in the open ocean zone. The elevated levels of dissolved iron contained in WDW can be introduced into the mixed layer via turbulent diapycnal mixing (Tagliabue et al., 2014). Diapycnal mixing may be occurring in this region via the action of the Antarctic Slope Front (Moreau et al., 2023), which is evidenced in these results by deepening isopycnals across the 6°E transect (**Figure 3a** and **b**). Indeed, a dense, annually recurring bloom associated with this front is attributed to hydrothermally derived iron from upwelled WDW, as indicated by anomalously high helium isotopic ratios (Moreau et al., 2023).

Altogether, the open ocean and coastal and polynya zones with the highest Chl *a* and NCP and lowest fCO_2 also had high meltwater fractions in the upper 100 m of the water column. The open ocean and coastal and polynya zones were presumably the zones with the highest potential photosynthetically available radiation in the water column. Based on literature estimates from similar latitudes and times of the productive season, light levels in these zones were expected to be above minimum light threshold for primary production (Moreau et al., 2010; Moreau et al., 2015). Light availability was thus more likely to be sufficient for bloom development in these zones as compared to the ice edge and pack ice zones. Bloom development in these zones also suggests sufficient iron provision, and meltwater fractions indicate that iron was more likely to be sea-ice derived in the open ocean and glacially derived in the coastal and polynya zone. The spatiotemporal coupling of increased light and iron availability related to sea-ice melting indicates the critical role of sea ice in fostering bloom conditions in the Southern Ocean, though disentangling the specific contribution of each growth-limiting factor is beyond the scope of this study. The inability of multivariate statistical analysis to accurately account for more than 40% of the variance in the data points to the simultaneous influence of several environmental drivers, further underlining the inherent limitations of this study. Additional research focused on light and iron concentrations in relationship to phytoplankton biomass during sea-ice melt is warranted to gain a better understanding of these complex dynamics.

4.3. Seasonal succession of phytoplankton communities

To elucidate the impacts of sea-ice melt on species succession, the results of this transect study may be considered as a timelapse of the sea-ice melt season, with the southern pack ice zone (Stations 12–17, 19) representing early spring conditions and the northern open ocean zone (Station 1) representing more summer-like conditions. Within this framework, we observed a phytoplankton bloom with greater abundance of flagellate species in the early spring (pack ice) zone and a dominance of diatoms in the summer (open ocean) zone (**Figure 6**). Following the assumption that similar ice algae and phytoplankton community successions take place throughout this space-limited area, this observed species succession thus adheres to an excepted phenology where sea ice is seeding the phytoplankton bloom (van Leeuwe et al., 2020; Kauko et al., 2022). van Leeuwe et al. (2022) describe that the link between sea-ice algal and pelagic blooms begins with an initial increase in ice-associated flagellate species, especially *Phaeocystis antarctica* and *Pyramimonas* spp., both of which were the dominating species observed in the pack ice zone of this study. Additionally, Lannuzel et al. (2013) documented *P. antarctica* as a species of ice algae likely to have seeded phytoplankton growth in their ship-based microcosm experiments. In these instances, the prevalence of flagellates during initial seeding phases is thought to be a result of their high plasticity for sea-ice and pelagic environments, whereas obligate shade-adapted pennate diatoms that dominate bottom-ice communities are less capable of such acclimation (Kropuenske et al., 2010; van Leeuwe et al., 2020).

In transition toward typical summer phytoplankton communities, algal blooms in the Southern Ocean are increasingly characterized by diatoms that respond quickly to increases in light and sea surface temperatures (van Leeuwe et al., 2020). The open ocean zone is then most representative of summertime environmental conditions, as light would have been most readily available and sea surface temperatures highest in this zone, compared to others in the study area (**Figure 2a**). This more advanced bloom phase is reflected in the community composition by a high abundance of diatoms, especially of the pennate diatom genus *Fragilariopsis*. Although species of *Fragilariopsis* are known to inhabit both sea ice and seawater (e.g., Lizotte, 2001), they are not typically regarded as the species that seed pelagic blooms. Rather, large blooms in the Southern Ocean are more commonly formed by centric diatom genera, such as *Thalassiosira* and *Chaetoceros* (Rozema et al., 2017; van Leeuwe et al., 2020; Kauko et al., 2022).

An intermediate step in the transition from spring to summer communities is observed in the ice edge zone in this dataset, where the community is 36.1% diatoms and 62.3% flagellates. The high contribution of heterotrophic choanoflagellates at the ice edge is consistent with previous findings of summer surface communities in Antarctic pack ice (**Figure 6**; Archer et al., 1996), which could be interpreted as a mixed community of released sympagic cells and emerging phytoplankton. Despite the evident impact of sea ice on phytoplankton growing conditions, the link between sympagic and pelagic algal communities remains unproven here and in the literature (e.g., Selz et al., 2018) and, as frequently found, sea-ice algae are no longer viable once released into the water column (Arrigo, 2014; van Leeuwe et al., 2018).

5. Conclusion

The biogeochemical growth conditions for phytoplankton in the Southern Ocean SIZ are impacted by the seasonal process of sea-ice melting, which results in high production and disproportionately low fCO_2. Our data suggest that the distribution of the phytoplankton bloom within the Kong Håkon VII Hav SIZ is most likely constrained primarily by the expected increases in light and iron availability associated with sea-ice melting. The most concentrated phytoplankton blooms were observed in the open ocean and coastal and polynya zones where sea-ice concentration was the lowest and not a probable cause of light limitation. Comparatively, in the most ice-covered zones (ice edge and pack ice zones) productivity was relatively low and light was more likely limited during the campaign. Potential sources of iron to support phytoplankton growth in the area were distinct between study zones. In the open ocean zone, high sea-ice meltwater fractions support that earlier iron provision by sea ice was important, while high meteoric meltwater fractions indicate that glacial sources were more relevant in the coastal and polynya zone. Hydrothermally derived iron from upwelled WDW may possibly have contributed to iron supply in the open ocean zone. The distribution of phytoplankton species across the entire study area showed a community succession consistent with a bloom progression linked to sea-ice melt. An early bloom phase possibly related to sea-ice seeding was observed in the pack ice zone, where the flagellate species *Pyramimonas* sp. and *Phaeocystis antarctica* were most dominant. A later season (early summer) bloom phase was observed in the open ocean zone where diatom cells were most dominant. Taxonomic composition data supported the POC:Chl *a* ratios, which were lowest in the pack ice and highest in the open ocean zone, also suggesting an early phase bloom in the pack ice zone and an advanced stage bloom in the open ocean zone. With Southern Ocean sea ice already in rapid decline and summertime extents expected to decrease between 29% and 90% by the end of the century (Roach et al., 2020; Purich and Doddridge, 2023), we suggest that processes associated with sea-ice melting will play a larger role in governing future phytoplankton bloom dynamics. In tandem, the dynamics of the Southern Ocean biological carbon pump are changing faster than current models are able to predict (Thomalla et al., 2023), rendering direct observations of this process highly relevant to predicting the fate of the Southern Ocean in the global climate system.

Data accessibility statement

The biogeochemical data used in this manuscript are available at http://doi.org/10.21334/npolar.2024.11d6598e. The taxonomy data used in this manuscript are available at http://doi.org/10.21334/npolar.2024.6161cdf5. Data from DIC and TA measurements are available at http://DOI.org/10.21334/npolar.2023.1da0e194. Satellite data used in this manuscript were accessed from http://navigator.eumetsat.int/product/EO:EUM:DAT:DMSP:OSI-401-B and http://nsidc.org/data/g10013/versions/1.

Supplemental files

The supplemental files for this article can be found as follows:

Figures S1–S2. Table S1. Docx.

Acknowledgments

Special thanks to Kristen Fossan (NPI), Vår Dundas (University of Bergen), and Julius Lauber (NPI) for participating in data acquisition for this manuscript. PC thanks Research Foundation Flanders (FWO) Hercules Program for IRMS purchase and VUB Strategic Research Program. The authors thank Dr Hannah Joy-Warren and an anonymous reviewer for their constructive revisions which improved the quality of the article.

Funding

The authors would like to thank the U.S.-Norway Fulbright Foundation for enabling a year of polar study at NPI and UiT for ML. Support for this project comes from the Norwegian Polar Institute Troll Transect program. This work is contribution to the RCN BREATHE (Bottom sea ice Respiration and nutrient Exchanges Assessed for THE Arctic, 325405) project, the RCN I-CRYME (Impact of CRYosphere Melting on Southern Ocean Ecosystems and biogeochemical cycles, 11993) project, and the RCN iC3 (Centre for ice, Cryosphere, Carbon and Climate, 332635) Center of Excellence project.

Competing interests

None declared.

Author contributions

Contributed to conception and design: ML, SM, KC.

Contributed to acquisition of data: SM, TH.

Contributed to analysis and interpretation of data: All authors.

Drafted and/or revised the manuscript: All authors.

Approved the submitted version for publication: All authors.

References

Alkire, MB, **Riser, S.** 2023. Net community production in the Argentine Basin estimated from nitrate drawdown using biogeochemical Argo floats. *Journal of Geophysical Research: Oceans* **128**(8): e2023JC

019858. DOI: http://dx.doi.org/10.1029/2023JC019858.

Archer, SD, **Leakey, RJG**, **Burkill, PH**, **Sleigh, MA**, **Appleby, CJ.** 1996. Microbial ecology of sea ice at a coastal Antarctic site: Community composition, biomass and temporal change. *Marine Ecology Progress Series* **135**: 179–195. DOI: http://dx.doi.org/10.3354/meps135179.

Arrigo, KR. 2014. Sea ice ecosystems. *Annual Review of Marine Science* **6**: 439–467. DOI: http://dx.doi.org/10.1146/annurev-marine-010213-135103.

Arrigo, KR, **van Dijken, GL**, **Bushinsky, S.** 2008. Primary production in the Southern Ocean, 1997–2006. *Journal of Geophysical Research: Oceans* **113**(C8): 2156–2202. DOI: http://dx.doi.org/10.1029/2007JC004551.

Behrenfeld, MJ, **Hu, Y**, **O'Malley, RT**, **Boss, ES**, **Hostetler, CA**, **Siegel, DA**, **Sarmiento, JL**, **Schulien, J**, **Hair, JW**, **Lu, X**, **Rodier, S**, **Scarino, AJ.** 2017. Annual boom-bust cycles of polar phytoplankton biomass revealed by space-based lidar. *Nature Geoscience* **10**: 118–122. DOI: http://dx.doi.org/10.1038/ngeo2861.

Beitsch, A, **Kern, S**, **Kaleschke, L.** 2015. Comparison of SSM/I and AMSR-E sea ice concentrations with ASPeCt ship observations around Antarctica. *IEEE Transactions on Geoscience and Remote Sensing* **53**(4): 1985–1996. DOI: http://dx.doi.org/10.1109/TGRS.2014.2351497.

Boyd, PW, **Watson, AJ**, **Law, CS**, **Abraham, ER**, **Trull, T**, **Murdoch, R**, **Bakker, DCE**, **Bowie, AR**, **Buesseler, KO**, **Chang, H**, **Charette, M**, **Croot, P**, **Downing, K**, **Frew, R**, **Gall, M**, **Hadfield, M**, **Hall, J**, **Harvey, M**, **Jameson, G**, **LaRoche, J**, **Liddicoat, M**, **Ling, R**, **Maldonado, MT**, **McKay, RM**, **Nodder, S**, **Pickmere, S**, **Pridmore, R**, **Rintoul, S**, **Safi, K**, **Sutton, P**, **Strzepek, R**, **Tanneberger, K**, **Turner, S**, **Waite, A**, **Zeldis, J**. 2000. A mesoscale phytoplankton bloom in the polar Southern Ocean stimulated by iron fertilization. *Nature* **407**(6805): 695–702. DOI: http://dx.doi.org/10.1038/35037500.

Cefarelli, A, **Ferrario, ME**, **Almandoz, G**, **Atencio, AG**, **Akselman, R**, **Vernet, M.** 2010. Diversity of the diatom genus *Fragilariopsis* in Argentine Sea and Antarctic waters: Morphology, distribution and abundance. *Polar Biology* **33**: 1463–1484. DOI: http://dx.doi.org/10.1007/s00300-010-0794-z.

Chierici, M, **Fransson, A**, **Turner, DR**, **Pakhomov, EA**, **Froneman, PW.** 2004. Variability in pH, fCO_2, oxygen and flux of CO_2 in the surface water along a transect in the Atlantic sector of the Southern Ocean. *Deep-Sea Research Part II: Topical Studies in Oceanography* **51**(22–24): 2773–2787. DOI: http://dx.doi.org/10.1016/j.dsr2.2001.03.002.

Corkill, M, **Moreau, S**, **Janssens, J**, **Fraser, AD**, **Heil, P**, **Tison, J-L**, **Cougnan, EA**, **Genovese, C**, **Kimura, N**, **Meiners, KM**, **Wongpan, P**, **Lannuzel, D.** 2023. Physical and biogeochemical properties of rotten East Antarctic summer sea ice. *Journal of Geophysical Research: Oceans* **128**(2): e2022JC018875. DOI: http://dx.doi.org/10.1029/2022JC018875.

Davidson, AT, **Scott, FJ**, **Nash, GV**, **Wright, SW**, **Raymond, B.** 2010. Physical and biological control of protistan community composition, distribution and abundance in the seasonal ice zone of the Southern Ocean between 30 and 80°E. *Deep Sea Research Part II: Topical Studies in Oceanography* **57**(9–10): 828–848. DOI: http://dx.doi.org/10.1016/j.dsr2.2009.02.011.

de Baar, HJW, **de Jong, JTM**, **Bakker, DCE**, **Löscher, BM**, **Veth, C**, **Bathmann, U**, **Smetacek, V.** 1995. Importance of iron for plankton blooms and carbon dioxide drawdown in the Southern Ocean. *Nature* **373**: 412–415. DOI: http://dx.doi.org/10.1038/373412a0.

Death, R, **Wadham, JL**, **Monteiro, F**, **Le Brocq, AM**, **Tranter, M**, **Ridgwell, A**, **Dutkiewicz, S**, **Raiswell, R.** 2014. Antarctic ice sheet fertilises the Southern Ocean. *Biogeosciences* **11**(10): 2635–2643. DOI: http://dx.doi.org/10.5194/bg-11-2635-2014.

Deppeler, SL, **Davidson, AT.** 2017. Southern Ocean phytoplankton in a changing climate. *Frontiers in Marine Science* **4**: 40. DOI: http://dx.doi.org/10.3389/fmars.2017.00040.

Dickson, A. 2001. Reference materials for oceanic CO_2 measurements. *Oceanography* **14**: 21–22.

Dickson, AG. 1990. Thermodynamics of the dissociation of boric acid in synthetic seawater from 273.15 to 318.15 K. *Deep Sea Research Part A. Oceanographic Research Papers* **37**(5): 755–766. DOI: http://dx.doi.org/10.1016/0198-0149(90)90004-F.

Dickson, AG, **Millero, FJ.** 1987. A comparison of the equilibrium constants for the dissociation of carbonic acid in seawater media. *Deep Sea Research Part A. Oceanographic Research Papers* **34**(10): 1733–1743. DOI: http://dx.doi.org/10.1016/0198-0149(87)90021-5.

Dickson, AG, **Sabine, CL**, **Chrstian, JR.** 2007. *Guide to best practices for CO_2 measurements*. British Columbia, Canada: North Pacific Marine Science Organization.

Dierssen, HM, **Vernet, M**, **Smith, RC.** 2000. Optimizing models for remotely estimating primary production in Antarctic coastal waters. *Antarctic Science* **12**(1): 20–32. DOI: http://dx.doi.org/10.1017/S0954102000000043.

Dinniman, MS, **St-Laurent, P**, **Arrigo, KR**, **Hofmann, EE**, **van Dijken, GL.** 2020. Analysis of iron sources in Antarctic continental shelf waters. *Journal of Geophysical Research: Oceans* **125**(5): e2019JC015736. DOI: http://dx.doi.org/10.1029/2019JC015736.

Douglas, CC, **Briggs, N**, **Brown, P**, **MacGilchrist, G**, **Naveira Garabato, A.** 2023. Exploring the relationship between sea-ice and primary production in the Weddell Gyre using satellite and Argo-float data. *EGUsphere* **2023**: 1–28. DOI: http://dx.doi.org/10.5194/egusphere-2023-1068.

Duprat, LPAM, **Bigg, GR**, **Wilton, DJ.** 2016. Enhanced Southern Ocean marine productivity due to fertilization by giant icebergs. *Nature Geoscience* **9**(3):

219–221. DOI: http://dx.doi.org/10.1038/ngeo2633.

Edler, L, **Elbrächter, M.** 2010. The Utermöhl method for quantitative phytoplankton analysis, in Karlson, B, Cusack, C, Bresnan, E eds., *Microscopic and molecular methods for quantitative phytoplankton analysis*. Paris, France: Intergovernmental Oceanographic Commission of UNESCO: 13–20.

Epstein, S, **Mayeda, T.** 1953. Variation of O^{18} content of waters from natural sources. *Geochimica et Cosmochimica Acta* **4**(5): 213–224. DOI: http://dx.doi.org/10.1016/0016-7037(53)90051-9.

Fitch, DT, **Moore, JK.** 2007. Wind speed influence on phytoplankton bloom dynamics in the Southern Ocean Marginal Ice Zone. *Journal of Geophysical Research: Oceans* **112**(C8). DOI: http://dx.doi.org/10.1029/2006JC004061.

Fransson, A, **Chierici, M**, **Anderson, LG.** 2004b. Diurnal variability in the oceanic carbon dioxide system and oxygen in the Southern Ocean surface water. *Deep-Sea Research Part II: Topical Studies in Oceanography* **51**(22–24): 2827–2839. DOI: http://dx.doi.org/10.1016/j.dsr2.2001.01.001.

Fransson, A, **Chierici, M**, **Anderson, L**, **David, R.** 2004a. Transformation of carbon and oxygen in the surface layer of the eastern Atlantic sector of the Southern Ocean. *Deep-Sea Research Part II: Topical Studies in Oceanography* **51**(22–24): 2757–2772. DOI: http://dx.doi.org/10.1016/j.dsr2.2001.12.001.

Frölicher, TL, **Sarmiento, JL**, **Paynter, DJ**, **Dunne, JP**, **Krasting, JP**, **Winton, M.** 2015. Dominance of the Southern Ocean in anthropogenic carbon and heat uptake in CMIP5 models. *Journal of Climate* **28**(2): 862–886. DOI: http://dx.doi.org/10.1175/JCLI-D-14-00117.1.

Gerringa, LJA, **Alderkamp, A-C**, **Laan, P**, **Thuróczy, C-E**, **De Baar, HJW**, **Mills, MM**, **van Dijken, GL**, **van Haren, H**, **Arrigo, KR.** 2012. Iron from melting glaciers fuels the phytoplankton blooms in Amundsen Sea (Southern Ocean): Iron biogeochemistry. *Deep Sea Research Part II: Topic Studies in Oceanography* **71–76**(15): 16–31. DOI: http://dx.doi.org/10.1016/j.dsr2.2012.03.007.

Grasshof, K, **Ehrhardt, M**, **Kremling, K.** 1983. *Methods of seawater analysis*. Weinheim, Germany: Verlag Chemie.

Gregor, L, **Lebehot, AD**, **Kok, S**, **Scheel Monteiro, PM.** 2019. A comparative assessment of the uncertainties of global surface ocean CO_2 estimates using a machine-learning ensemble (CSIR-ML6 version 2019a)—Have we hit the wall? *Geoscientific Model Development* **12**(12): 5113–5136. DOI: http://dx.doi.org/10.5194/gmd-12-5113-2019.

Gruber, N, **Landschützer, P**, **Lovenduski, NS.** 2019. The variable Southern Ocean carbon sink. *Annual Review of Marine Science* **11**(1): 159–186. DOI: http://dx.doi.org/10.1146/annurev-marine-121916-063407.

Hague, M, **Vichi, M.** 2021. Southern Ocean Biogeochemical Argo detect under-ice phytoplankton growth before sea ice retreat. *Biogeosciences* **18**(1): 25–38. DOI: http://dx.doi.org/10.5194/bg-18-25-2021.

Harmon, C. 1961. Isotopic variations in meteoric waters. *Science* **133**(3465): 1702–1703. DOI: http://dx.doi.org/10.1126/science.133.3465.1702.

Hattermann, T. 2018. Antarctic thermocline dynamics along a narrow shelf with easterly winds. *Journal of Physical Oceanography* **48**(10): 2419–2443. DOI: http://dx.doi.org/10.1175/JPO-D-18-0064.1.

Herraiz-Borreguero, L, **Lannuzel, D**, **van der Merwe, P**, **Treverrow, A**, **Pedro, JB.** 2016. Large flux of iron from the Amery Ice Shelf marine ice to Prydz Bay, East Antarctica. *Journal of Geophysical Research: Oceans* **121**(8): 6009–6020. DOI: http://dx.doi.org/10.1002/2016JC011687.

Holm-Hansen, O, **Riemann, B.** 1978. Chlorophyll a determination: Improvements in methodology. *Oikos* **30**(3): 438–447. DOI: http://dx.doi.org/10.2307/3543338.

Horvat, C, **Bisson, K**, **Seabrook, S**, **Cristi, A**, **Matthes, LC.** 2022. Evidence of phytoplankton blooms under Antarctic Sea ice. *Frontiers in Marine Science* **9**. DOI: http://dx.doi.org/10.3389/fmars.2022.942799.

IOC SaI. 2010. The International Thermodynamic Equation of Seawater—2010 (TEOS-10): Calculation and use of thermodynamic properties. Paris, France: UNESCO. (Manuals and Guides No. 56).

Jickells, T, **Moore, CM.** 2015. The importance of atmospheric deposition for ocean productivity. *Annual Review of Ecology, Evolution, and Systematics* **46**(1): 481–501. DOI: http://dx.doi.org/10.1146/annurev-ecolsys-112414-054118.

Johansen, JR, **Fryxell, GA.** 1985. The genus *Thalassiosira* (Bacillariophyceae): Studies on species occurring south of the Antarctic Convergence Zone. *Phycologia* **24**(2): 155–179. DOI: http://dx.doi.org/10.2216/i0031-8884-24-2-155.1.

Johnson, KM, **Sieburth, JMcN**, **leB Williams, PJ**, **Brändström, L.** 1987. Coulometric total carbon dioxide analysis for marine studies: Automation and calibration. *Marine Chemistry* **21**(2): 117–133. DOI: http://dx.doi.org/10.1016/0304-4203(87)90033-8.

Joy-Warren, HL, **van Dijken, GL**, **Alderkamp, A-C**, **Leventer, A**, **Lewis, KM**, **Selz, V**, **Lowry, KE**, **van de Poll, W**, **Arrigo, KR.** 2019. Light is the primary driver of early season phytoplankton production along the Western Antarctic Peninsula. *Journal of Geophysical Research: Oceans* **124**(11): 7375–7399. DOI: http://dx.doi.org/10.1029/2019JC015295.

Kang, S-H, **Kang, J-S**, **Lee, S**, **Chung, KH**, **Kim, D**, **Park, MG.** 2001. Antarctic phytoplankton assemblages in the marginal ice zone of the northwestern Weddell Sea. *Journal of Plankton Research* **23**(4): 333–352. DOI: http://dx.doi.org/10.1093/plankt/23.4.333.

Kauko, HM, **Assmy, P**, **Peeken, I**, **Różańska, M**, **Wiktor, JM**, **Bratbak, G**, **Singh, A**, **Ryan-Keogh, TJ**, **Moreau, S.** 2022. First phytoplankton community assessment of the Kong Håkon VII Hav, Southern Ocean during austral autumn. *Biogeosciences*

Discussions **19**(23): 1–60. DOI: http://dx.doi.org/10.5194/bg-2022-45.

Kauko, HM, **Hattermann, T**, **Ryan-Keogh, T**, **Singh, A**, **de Steur, L**, **Fransson, A**, **Chierici, M**, **Falkenhaug, T**, **Hallfredsson, EH**, **Bratbak, G**, **Tsagaraki, T**, **Berge, T**, **Zhou, Q**, **Moreau, S.** 2021. Phenology and environmental control of phytoplankton blooms in the Kong Håkon VII Hav in the Southern Ocean. *Frontiers in Marine Science* **8**. DOI: http://dx.doi.org/10.3389/fmars.2021.623856.

Keppler, L, **Landschützer, P**, **Gruber, N**, **Lauvset, SK**, **Stemmler, I.** 2020. Seasonal carbon dynamics in the near-global ocean. *Global Biogeochemical Cycles* **34**(12): e2020GB006571. DOI: http://dx.doi.org/10.1029/2020GB006571.

Krell, A, **Schnack-Schiel, SB**, **Thomas, DN**, **Kattner, G**, **Zipan, W**, **Dieckmann, GS.** 2005. Phytoplankton dynamics in relation to hydrography, nutrients and zooplankton at the onset of sea ice formation in the eastern Weddell Sea (Antarctica). *Polar Biology* **28**(9): 700–713. DOI: http://dx.doi.org/10.1007/s00300-005-0733-6.

Kropuenske, LR, **Mills, MM**, **van Dijken, GL**, **Alderkamp, AC**, **Berg, GM**, **Robinson, DH**, **Welschmeyer, NA**, **Arrigo, KR.** 2010. Strategies and rates of photoacclimation in two major Southern Ocean phytoplankton taxa: *Phaeocystis antarctica* (Haptophyte) and *Fragilariopsis cylindrus* (Bacillariophyceae). *Journal of Phycology* **46**(6): 1138–1151. DOI: http://dx.doi.org/10.1111/j.1529-8817.2010.00922.x.

Lancelot, C, **Billen, G**, **Veth, C**, **Becquevort, S**, **Mathot, S.** 1991. Modelling carbon cycling through phytoplankton and microbes in the Scotia–Weddell Sea area during sea ice retreat. *Marine Chemistry* **35**(1–4): 305–324. DOI: http://dx.doi.org/10.1016/S0304-4203(09)90024-X.

Lannuzel, D, **Schoemann, V**, **Dumont, I**, **Content, M**, **de Jong, J**, **Tison, J-L**, **Delille, B**, **Becquevort, S.** 2013. Effect of melting Antarctic Sea ice on the fate of microbial communities studied in microcosms. *Polar Biology* **36**(10): 1483–1497. DOI: http://dx.doi.org/10.1007/s00300-013-1368-7.

Lannuzel, D, **Vancoppenolle, M**, **van der Merwe, P**, **de Jong, J**, **Meiners, KM**, **Grotti, M**, **Nischioka, J**, **Schoermann, V.** 2016. Iron in sea ice: Review and new insights. *Elementa: Science of the Anthropocene* **4**: 000130. DOI: http://dx.doi.org/10.12952/journal.elementa.000130.

Lavergne, T, **Sørensen, AM**, **Kern, S**, **Tonboe, R**, **Notz, D**, **Aaboe, S**, **Bell, L**, **Dybkjær, G**, **Eastwood, S**, **Gabarro, C**, **Heygster, G**, **Killie, MA**, **Brandt Kreiner, M**, **Lavelle, J**, **Saldo, R**, **Sandve, S**, **Toudal Pederson, L.** 2019. Version 2 of the EUMETSAT OSI SAF and ESA CCI sea-ice concentration climate data records. *The Cryosphere* **13**(1): 49–78. DOI: http://dx.doi.org/10.5194/tc-13-49-2019.

Liénart, C, **Susperregui, N**, **Rouaud, V**, **Cavalheiro, J**, **David, V**, **Del Amo, Y**, **Duran, R**, **Lauga, B**, **Monperrus, M**, **Pigot, T**, **Bichon, S**, **Charlier, K**, **Savoye, N.** 2016. Dynamics of particulate organic matter in a coastal system characterized by the occurrence of marine mucilage—A stable isotope study. *Journal of Sea Research* **116**: 12–22. DOI: http://dx.doi.org/10.1016/j.seares.2016.08.001.

Lizotte, MP. 2001. The contributions of sea ice algae to Antarctic marine primary production. *American Zoologist* **41**(1): 57–73. DOI: http://dx.doi.org/10.1093/icb/41.1.57.

Marinov, I, **Gnanadesikan, A**, **Toggweiler, JR**, **Sarmiento, JL.** 2006. The Southern Ocean biogeochemical divide. *Nature* **441**: 964–967. DOI: http://dx.doi.org/10.1038/nature04883.

Martin, JH, **Gordon, RM**, **Fitzwater, SE.** 1990. Iron in Antarctic waters. *Nature* **345**: 156–158. DOI: http://dx.doi.org/10.1038/345156a0.

Massom, RA, **Eicken, H**, **Haas, C**, **Jeffries, MO**, **Drinkwater, MR**, **Sturm, M**, **Worby, AP**, **Wu, X**, **Lytle, VI**, **Ushio, S**, **Morris, K**, **Reid, PA**, **Warren, SG**, **Allison, I.** 2001. Snow on Antarctic sea ice. *Reviews of Geophysics* **39**(3): 413–445. DOI: http://dx.doi.org/10.1029/2000rg000085.

Matsuoka, K, **Skoglund, A**, **Roth, G**, **de Pomereu, J**, **Griffiths, H**, **Headland, R**, **Herried, B**, **Katsumata, K**, **Le Brocq, A**, **Licht, K**, **Morgan, F**, **Neff, PD**, **Ritz, C**, **Scheinert, M**, **Tamura, T**, **Van de Putte, A**, **van den Broeke, M**, **von Deschwanden, A**, **Deschamps-Berger, C**, **Van Liefferinge, B**, **Melvær, Y.** 2021. Quantarctica, an integrated mapping environment for Antarctica, the Southern Ocean, and sub-Antarctic islands. *Environmental Modelling & Software* **140**: 105015. DOI: http://dx.doi.org/10.1016/j.envsoft.2021.105015.

Mdutyana, M, **Thomalla, SJ**, **Philibert, R**, **Ward, BB**, **Fawcett, SE.** 2020. The seasonal cycle of nitrogen uptake and nitrification in the Atlantic sector of the Southern Ocean. *Global Biogeochemical Cycles* **34**(7): e2019GB006363. DOI: http://dx.doi.org/10.1029/2019GB006363.

Mehrbach, C, **Culberson, CH**, **Hawley, JE**, **Pytkowicz, RN.** 1973. Measurement of the apparent dissociation constants of carbonic acid in seawater at atmospheric pressure. *Limnology and Oceanography* **18**(6): 897–907. DOI: http://dx.doi.org/10.4319/lo.1973.18.6.0897.

Meredith, MP, **Venables, HJ**, **Clarke, A**, **Ducklow, HW**, **Erickson, M**, **Leng, MJ**, **Lenaerts, JTM**, **van den Broeke, MR**. 2013. The freshwater system west of the Antarctic Peninsula: Spatial and temporal changes. *Journal of Climate* **26**(5): 1669–1684. DOI: http://dx.doi.org/10.1175/JCLI-D-12-00246.1.

Moore, CM, **Mills, MM**, **Arrigo, KR**, **Berman-Frank, I**, **Bopp, L**, **Boyd, PW**, **Galbraith, ED**, **Geider, RJ**, **Guieu, C**, **Jaccard, SL**, **Jickells, TD**, **La Roche, J**, **Lenton, TM**, **Mahowald, NM**, **Marñón, E**, **Marinov, I**, **Moore, JK**, **Nakatsuka, T**, **Oschlies, A**, **Saito, MA**, **Thingstad, TF**, **Tusda, A**, **Ulloa, O.** 2013. Processes and patterns of oceanic nutrient limitation. *Nature Geoscience* **6**: 701–710. DOI: http://dx.doi.org/10.1038/NGEO1765.

Moran, SB, **Charette, MA**, **Pike, SM**, **Wicklund, CA.** 1999. Differences in seawater particulate organic carbon concentration in samples collected using small- and large-volume methods: The importance of DOC adsorption to the filter blank. *Marine Chemistry* **67**(1–2): 33–42. DOI: http://dx.doi.org/10.1016/S0304-4203(99)00047-X.

Moreau, S, **di Fiori, E**, **Schloss, IR**, **Almandoz, GO**, **Esteves, JL**, **Papparazzo, FE**, **Ferreyra, GA.** 2013. The role of phytoplankton composition and microbial community metabolism in sea–air ΔpCO_2 variation in the Weddell Sea. *Deep Sea Research Part I: Oceanographic Research Papers* **82**: 44–59. DOI: http://dx.doi.org/10.1016/j.dsr.2013.07.010.

Moreau, S, **Ferreyra, GA**, **Mercier, B**, **Lemarchand, K**, **Lionard, M**, **Roy, S**, **Mostajir, B**, **Roy, S**, **van Hardenberg, B**, **Demers, S.** 2010. Variability of the microbial community in the western Antarctic Peninsula from late fall to spring during a low ice cover year. *Polar Biology* **33**: 1599–1614. DOI: http://dx.doi.org/10.1007/s00300-010-0806-z.

Moreau, S, **Hattermann, T**, **de Steur, L**, **Kauko, HM**, **Ahonen, H**, **Ardelan, M**, **Assmy, P**, **Chierici, M**, **Descamps, S**, **Dinter, T**, **Falkenhaug, T**, **Fransson, A**, **Grønningsæter, E**, **Hallfredsson, EH**, **Huhn, O**, **Lebrun, A**, **Lowther, A**, **Lübcker, N**, **Monteiro, P**, **Peekan, I**, **Roychoudhury, A**, **Różańska, M**, **Ryan-Keogh, T**, **Sanchez, N**, **Singh, A**, **Simonsen, JH**, **Steiger, N**, **Thomalla, SJ**, **van Tonder, A**, **Wiktor, JM**, **Steen, H.** 2023. Wind-driven upwelling of iron sustains dense blooms and food webs in the eastern Weddell Gyre. *Nature Communications* **14**(1): 1303. DOI: http://dx.doi.org/10.1038/s41467-023-36992-1.

Moreau, S, **Lannuzel, D**, **Janssens, J**, **Arroyo, MC**, **Corkill, M**, **Cougnon, E**, **Genovese, C**, **Legresy, B**, **Lenton, A**, **Puigorbé, V**, **Ratnarajah, L**, **Rintoul, S**, **Roca-Martí, M**, **Rosenberg, M**, **Shadwick, EH**, **Silvano, A**, **Strutton, PG**, **Tilbrook, B.** 2019. Sea ice meltwater and circumpolar deep water drive contrasting productivity in three Antarctic polynyas. *Journal of Geophysical Research: Oceans* **124**(5): 2943–2968. DOI: http://dx.doi.org/10.1029/2019JC015071.

Moreau, S, **Mostajir, B**, **Belanger, S**, **Schloos, IR**, **Vancoppenolle, M**, **Demers, S**, **Ferreyra, GA.** 2015. Climate change enhances primary production in the western Antarctic Peninsula. *Global Change Biology* **21**(6): 2191–2205. DOI: http://dx.doi.org/10.1111/gcb.12878.

Ogundare, MO, **Fransson, A**, **Chierici, M**, **Joubert, WR**, **Roychoudhury, AN.** 2021. Variability of sea-air carbon dioxide flux in autumn across the Weddell Gyre and offshore Dronning Maud Land in the Southern Ocean. *Frontiers in Marine Science* **7**: 614263. DOI: http://dx.doi.org/10.3389/fmars.2020.614263.

Öquist, GW, **Chow, WS**, **Anderson, JM.** 1992. Photoinhibition of photosynthesis represents a mechanism for the long-term regulation of photosystem II. *Planta* **186**: 450–460. DOI: http://dx.doi.org/10.1007/BF00195327.

OSI SAF. 2017. Global sea ice concentration (netCDF)—DMSP. EUMETSAT SAF on Ocean and Sea Ice. DOI: http://dx.doi.org/10.15770/EUM_SAF_OSI_NRT_2004.

Pierrot, D, **Lewis, E**, **Wallce, DWR**. 2006. MS Excel program developed for CO_2 system calculations. Oak Ridge, TN: ORNL/CDAIC-105 Carbon Dioxide Information Analsysis Center. DOI: http://dx.doi.org/10.3334/cdiac/otg.co2sys_xls_cdiac105a.

Purich, A, **Doddridge, EW.** 2023. Record low Antarctic Sea ice coverage indicates a new sea ice state. *Communications Earth & Environment* **4**(1): 314. DOI: http://dx.doi.org/10.1038/s43247-023-00961-9.

Ratnarajah, L, **Puigcorbé, V**, **Moreau, S**, **Roca-Martí, M**, **Janssens, J**, **Corkill, M**, **Duprat, L**, **Genovese, C**, **Lieser, J**, **Masqué, P**, **Lannuzel, D.** 2022. Distribution and export of particulate organic carbon in East Antarctic coastal polynyas. *Deep Sea Research Part I: Oceanographic Research Papers* **190**: 103899. DOI: http://dx.doi.org/10.1016/j.dsr.2022.103899.

Redfield, AC, **Ketchum, BH**, **Richards, FA.** 1963. The influence of organisms on the composition of sea-water, in Hill, MN ed., *The global coastal ocean* (vol. 2). Cambridge, MA: Harvard University Press: 26–77.

Roach, LA, **Dörr, J**, **Holmes, CR**, **Massonnet, F**, **Blockley, EW**, **Notz, D**, **Rackow, T**, **Raphael, MN**, **O'Farrell, SP**, **Bailey, DA**, **Bitz, CM.** 2020. Antarctic sea ice area in CMIP6. *Geophysical Research Letters* **47**(9). DOI: http://dx.doi.org/10.1029/2019GL086729.

Rozema, PD, **Biggs, T**, **Sprong, PAA**, **Buma, AGJ**, **Venables, HJ**, **Evans, C**, **Meredith, MP**, **Bolhuis, H.** 2017. Summer microbial community composition governed by upper-ocean stratification and nutrient availability in northern Marguerite Bay, Antarctica. *Deep Sea Research Part II: Topical Studies in Oceanography* **139**: 151–166. DOI: http://dx.doi.org/10.1016/j.dsr2.2016.11.016.

Schandelmeier, L, **Alexander, V.** 1981. An analysis of the influence of ice on spring phytoplankton population structure in the southeast Bering Sea. *Limnology and Oceanography* **26**(5): 935–943. DOI: http://dx.doi.org/10.4319/lo.1981.26.5.0935.

Scott, FJ, **Marchant, HJ.** 2005. *Antarctic marine protists*. Kingston, Canada: Australian Biological Resources Study and Australian Antarctic Division.

Selz, V, **Lowry, KE**, **Lewis, KM**, **Joy-Warren, HL**, **van de Poll, W**, **Nirmel, S**, **Tong, A**, **Arrigo, KR.** 2018. Distribution of *Phaeocystis antarctica*-dominated sea ice algal communities and their potential to seed phytoplankton across the western Antarctic Peninsula in spring. *Marine Ecology Progress Series* **586**: 91–112. DOI: http://dx.doi.org/10.3354/meps12367.

Sherrell, RM, **Lagerström, ME**, **Forsch, KO**, **Stammerjohn, SE**, **Yager, PL.** 2015. Dynamics of dissolved iron and other bioactive trace metals (Mn, Ni, Cu, Zn) in the Amundsen Sea Polynya, Antarctica. *Elementa: Science of the Anthropocene* **3**: 000071. DOI: http://dx.doi.org/10.12952/journal.elementa.000071.

Silvano, A, **Rintoul, SR**, **Pena-Molino, B**, **Hobbs, WR**, **Van Wijk, E**, **Aoki, S**, **Tamura, T**, **Williams, GD.** 2018. Freshening by glacial meltwater enhances melting of ice shelves and reduces formation of Antarctic bottom water. *Science Advances* **4**(4). DOI: http://dx.doi.org/10.1126/sciadv.aap9467.

Singh, A, **Fietz, S**, **Thomalla, SJ**, **Sanchez, N**, **Ardelan, MV**, **Moreau, S**, **Kauko, HM**, **Fransson, A**, **Chierici, M**, **Samanta, S**, **Mtshali, TN**, **Roychoudhury, AN**, **Ryan-Keogh, TJ.** 2023. Absence of photophysiological response to iron addition in autumn phytoplankton in the Antarctic sea-ice zone. *Biogeosciences* **20**(14): 3073–3091. DOI: http://dx.doi.org/10.5194/bg-20-3073-2023.

Smith, WO, **Nelson, DM.** 1985. Phytoplankton bloom produced by a receding ice edge in the Ross sea: Spatial coherence with the density field. *Science* **227**(4683): 163–166. DOI: http://dx.doi.org/10.1126/science.227.4683.163.

Smith, WO Jr, **Nelson, DM.** 1986. Importance of ice edge phytoplankton production in the Southern Ocean. *BioScience* **36**(4): 251–257. DOI: http://dx.doi.org/10.2307/1310215.

Stammerjohn, SE, **Martinson, DG**, **Smith, RC**, **Yuan, X**, **Rind, D.** 2008. Trends in Antarctic annual sea ice retreat and advance and their relation to El Niño-Southern Oscillation and Southern Annular Mode variability. *Journal of Geophysical Research: Oceans* **113**(C3): 2156–2202. DOI: http://dx.doi.org/10.1029/2007JC004269.

Steiner, NS, **Bowman, J**, **Campbell, K**, **Chierici, M**, **Eronen-Rasimus, E**, **Flaradeu, M**, **Flores, H**, **Fransson, A**, **Herr, H**, **Insley, SJ**, **Kauko, HM**, **Lannuzel, D**, **Loseto, L**, **Lynnes, A**, **Majewski, A**, **Meiners, KM**, **Miller, LA**, **Michel, LN**, **Moreau, S**, **Nacke, M**, **Nomura, D**, **Tedesco, L**, **van Franeker, JA**, **van Leeuwe, MA**, **Wongpan, P.** 2021. Climate change impacts on sea-ice ecosystems and associated ecosystem services. *Elementa: Science of the Anthropocene* **9**(1): 00007. DOI: http://dx.doi.org/10.1525/elementa.2021.00007.

St-Laurent, P, **Yager, PL**, **Sherrell, RM**, **Stammerjohn, SE**, **Dinniman, MS.** 2017. Pathways and supply of dissolved iron in the Amundsen Sea (Antarctica). *Journal of Geophysical Research: Oceans* **122**(9): 7135–7162. DOI: http://dx.doi.org/10.1002/2017JC013162.

Szmytkowski, J, **Brunet, SMK**, **Tripathy, U**, **O'Brien, JA**, **Paige, MF**, **Steer, RP.** 2011. Photophysics and halide quenching of Soret-excited $ZnTPPS^{4-}$ in aqueous media. *Chemical Physics Letters* **501**(4–6): 278–282. DOI: http://dx.doi.org/10.1016/j.cplett.2010.11.010.

Tagliabue, A, **Sallee, J-B**, **Bowie, AR**, **Levy, M**, **Swart, S**, **Boyd, PW.** 2014. Surface-water iron supplies in the Southern Ocean sustained by deep winter mixing. *Nature Geoscience* **7**(4): 314–320. DOI: http://dx.doi.org/10.1038/ngeo2101.

Takahashi, T, **Olafsson, J**, **Goddard, JG**, **Chipman, DW**, **Sutherland, SC.** 1993. Seasonal variation of CO_2 and nutrients in the high-latitude surface oceans: A comparative study. *Global Biogeochemical Cycles* **7**(4): 843–878. DOI: http://dx.doi.org/10.1029/93GB02263.

Taylor, MH, **Losch, M**, **Bracher, A.** 2013. On the drivers of phytoplankton blooms in the Antarctic marginal ice zone: A modeling approach. *Journal of Geophysical Research: Oceans* **118**(1): 63–75. DOI: http://dx.doi.org/10.1029/2012JC008418.

Thomalla, SJ, **Gilbert Ogunkoya, A**, **Vichi, M**, **Swart, S.** 2017. Using optical sensors on gliders to estimate phytoplankton carbon concentrations and chlorophyll-to-carbon ratios in the Southern Ocean. *Frontiers in Marine Science* **4**. DOI: http://dx.doi.org/10.3389/fmars.2017.00034.

Thomalla, SJ, **Nicholson, S-A**, **Ryan-Keogh, TJ**, **Smith, ME.** 2023. Widespread changes in Southern Ocean phytoplankton blooms linked to climate drivers. *Nature Climate Change* **13**(9): 975–984. DOI: http://dx.doi.org/10.1038/s41558-023-01768-4.

Thomas, CR. 1997. *Identifying marine phytoplankton.* San Diego, CA: Academic Press.

Thompson, AF, **Stewart, AL**, **Spence, P**, **Heywood, KJ.** 2018. The Antarctic slope current in a changing climate. *Reviews of Geophysics* **56**(4): 741–770. DOI: http://dx.doi.org/10.1029/2018RG000624.

Tison, J-L, **Schwegmann, S**, **Dieckmann, G**, **Rintala, J-M**, **Meyer, H**, **Moreau, S**, **Vancoppenolle, M**, **Nomura, D**, **Engberg, S**, **Blomster, LJ**, **Hendricks, S**, **Uhlig, C**, **Luhtanen, A-M**, **de Jong, J**, **Janssens, J**, **Carnat, G**, **Zhou, J**, **Delille, B.** 2017. Biogeochemical impact of snow cover and cyclonic intrusions on the winter Weddell Sea ice pack. *Journal of Geophysical Research: Oceans* **122**(12): 9548–9571. DOI: http://dx.doi.org/10.1002/2017JC013288.

U.S. National Ice Center. 2022. U.S. National Ice Center Arctic and Antarctic Sea ice charts in SIGRID-3 format, version 1. G10013. DOI: http://dx.doi.org/10.7265/4B7S-RN93.

Utermöhl, H. 1958. Zur Vervollkommnung der quantitativen Phytoplankton-Methodik. *Internationale Vereinigung für Theoretische und Angewandte Limnologie: Mitteilungen* **9**(1): 1–38. DOI: http://dx.doi.org/10.1080/05384680.1958.11904091.

van Leeuwe, MA, **Fenton, M**, **Davey, E**, **Rintala, J-M**, **Jones, EM**, **Meredith, MP**, **Stefels, J.** 2022. On the phenology and seeding potential of sea-ice microalgal species. *Elementa: Science of the Anthropocene* **10**(1): 00029. DOI: http://dx.doi.org/10.1525/elementa.2021.00029.

van Leeuwe, MA, **Tedesco, L**, **Arrigo, KR**, **Assmy, P**, **Campbell, K**, **Meiners, KM**, **Rintala, J-M**, **Zelz, V**, **Thomas, DN**, **Stefels, J.** 2018. Microalgal community structure and primary production in Arctic and Antarctic Sea ice: A synthesis. *Elementa: Science of the Anthropocene* **6**: 4. DOI: http://dx.doi.org/10.1525/elementa.267.

van Leeuwe, MA, **Webb, AL**, **Venables, HJ**, **Visser, RJW**, **Meredith, MP**, **Elzenga, JTM**, **Stefels, J.** 2020. Annual patterns in phytoplankton phenology in Antarctic coastal waters explained by environmental

drivers. *Limnology and Oceanography* **65**(7): 1651–1668. DOI: http://dx.doi.org/10.1002/lno.11477.

Vernet, M, **Geibert, W**, **Hoppema, M**, **Brown, PJ**, **Haas, C**, **Hellmer, HH**, **Jokat, W**, **Jullion, L**, **Mazloff, M**, **Bakker, DCE**, **Brearley, JA**, **Croot, P**, **Hattermann, T**, **Hacuk, J**, **Hillenbrand, C-D**, **Hoppe, CJM**, **Huhn, O**, **Koch, BP**, **Lechtenfeld, OJ**, **Meredith, MP**, **Naveira Garabato, AC**, **Nöthig, E-M**, **Peeken, I**, **Rutgers van der Loeff, MM**, **Schmidtko, S**, **Schröder, VH**, **Strass, S**, **Torres-Valdés, S**, **Verdy, A**. 2019. The Weddell Gyre, Southern Ocean: Present knowledge and future challenges. *Reviews of Geophysics* **57**(3): 623–708. DOI: http://dx.doi.org/10.1029/2018RG000604.

von Berg, L, **Prend, CJ**, **Campbell, EC**, **Mazloff, MR**, **Talley, LD**, **Gille, ST.** 2020. Weddell Sea phytoplankton blooms modulated by sea ice variability and polynya formation. *Geophysical Research Letters* **47**(11). DOI: http://dx.doi.org/10.1029/2020GL087954.

WMO-IOC. 2004. SIGRID-3: A vector archive format for sea ice charts: Developed by the International Ice Charting Working Group's Ad Hoc Format Team for the WMO Global Digital Sea Ice Data Bank Project [dataset]. Geneva, Switzerland: WMO & IOC. JCOMM Technical Report No. 23.

WoRMS Editorial Board. 2024. World register of marine species. Available at http://www.marinespecies.org. Accessed January 11, 2024.

Wright, SW, **van den Enden, RL**, **Pearce, I**, **Davidson, AT**, **Scott, FJ**, **Westwood, KJ.** 2010. Phytoplankton community structure and stocks in the Southern Ocean (30–80°E) determined by CHEMTAX analysis of HPLC pigment signatures. *Deep Sea Research Part II: Topical Studies in Oceanography* **57**(9–10): 758–778. DOI: http://dx.doi.org/10.1016/j.dsr2.2009.06.015.

Xing, X, **Briggs, N**, **Boss, E**, **Claustre, H.** 2018. Improved correction for non-photochemical quenching of *in situ* chlorophyll fluorescence based on a synchronous irradiance profile. *Optics Express* **26**(19): 24734–24751. DOI: http://dx.doi.org/10.1364/OE.26.024734.

Zeebe, RE, **Wolf-Galdrow, D.** 2001. *CO_2 in seawater: Equilibrium, kinetics, isotopes*. Amsterdam, The Netherlands: Elsevier Science.

How to cite this article: Lenss, M, Moreau, S, Hattermann, T, Wiktor, J, Różańska, M, Claeys, P, Brion, N, Chierici, M, Fransson, A, Campbell, K. 2024. Phytoplankton bloom distribution and succession driven by sea-ice melt in the Kong Håkon VII Hav. *Elementa: Science of the Anthropocene* 12(1). DOI: https://doi.org/10.1525/elementa.2023.00122

Domain Editor-in-Chief: Jody W. Deming, University of Washington, Seattle, WA, USA

Associate Editor: Mathieu Ardyna, Stanford University, Stanford, CA, USA

Knowledge Domain: Ocean Science

Part of an Elementa Special Feature: Insights into Biogeochemical Exchange Processes at Sea Ice Interfaces (BEPSII-2)

Published: August 02, 2024 **Accepted:** June 12, 2024 **Submitted:** October 12, 2023

ELEMENTA Science of the Anthropocene

Elem Sci Anth is a peer-reviewed open access journal published by University of California Press.

OPEN ACCESS